OUKA
Osaka University Knowledge Archive

Title	Photofunctional nano-object network and its application
Author(s)	下村, 優
Citation	大阪大学, 2021, 博士論文
Version Type	VoR
URL	https://doi.org/10.18910/82281
rights	
Note	

Osaka University Knowledge Archive : OUKA

https://ir.library.osaka-u.ac.jp/

Osaka University

Photofunctional nano-object network and its application

Submitted to
Graduate School of Information Science and Technology
Osaka University

January 2021

Suguru SHIMOMURA

List of publications

Publications

[1] S. Shimomura, T. Nishimura, Y. Miyata, N. Tate, Y. Ogura, and J. Tanida, "Spectral and temporal optical signal generation using randomly distributed quantum dots," Optical Review **27**, 264–269 (2020) [Peer-reviewed].

[2] S. Shimomura, T. Nishimura, Y. Ogura, and J. Tanida, "Optical decomposition of DNA gel and modification of object mobility on micrometre scale," Scientific Reports **9**, 19858 (2019) [Peer-reviewed].

[3] S. Shimomura, T. Nishimura, Y. Ogura, and J. Tanida, "Photothermal fabrication of microscale patterned DNA hydrogels," Royal Society Open Science **5**, 171779 (2018) [Peer-reviewed].

Presentations

[1] S. Shimomura, T. Nishimura, J. Kozuka, Y. Miyata, S. Sakai, N. Tate, Y. Ogura, and J. Tanida, "Temporal signal generation using FRET-based quantum dot network for optical reservoir computing," Information Photonics 2020 (IP'20), F2.3 (2020) [Oral, peer-reviewed].

[2] S. Shimomura, T. Nishimura, Y. Ogura, and J. Tanida, "Object movement change in optical decomposition of DNA gels," The 9th Korea-Japan Workshop on Digital Holography and Information Photonics (DHIP2019), p18–15 (2019) [Poster].

[3] S. Shimomura, T. Nishimura, Y. Ogura, and J. Tanida, "Reversible transformation of DNA gels using light signals," The 5th Biomedical Imaging and Sensing Conference (BISC2019), JS–4–09 (2019) [Oral, peer-reviewed].

[4] S. Shimomura, T. Nishimura, Y. Miyata, N. Tate, Y. Ogura, and J. Tanida, "Energy transfer in quantum-dot network for optical reservoir computing," Information Photonics 2019 (IP2019), IP-1-05 (2019) [Oral, peer-reviewed].

[5] S. Shimomura, T. Nishimura, Y. Ogura, and J. Tanida, "Patterning of DNA hydrogels by photodecomposition with visible light," Microfluidics, BioMEMS, and Medical Microsystems XVII, SPIE BIOS 2019, 10875–22 (2019) [Oral, peer-reviewed].

[6] S. Shimomura, T. Nishimura, Y. Ogura, and J. Tanida, "Motion control of micrometer-sized object by photodecompotision of DNA hydrogels," The 24th International Conference on DNA Computing and Molecular Programming (DNA 24), P011 (2018) [Poster, peer-reviewed].

[7] S. Shimomura, T. Nishimura, Y. Ogura, and J. Tanida, "Quantitative evaluation of DNA hydrogel growth induced by light," The Twelfth Japan-Finland Joint Symposium on Optics in Engineering (OIE'17), P1 (2017) [Poster].

[8] S. Shimomura, T. Nishimura, Y. Ogura, and J. Tanida, "Optical fabrication of DNA hydrogel using quenchers," The 23rd International Conference on DNA Computing and Molecular Programming (DNA 23), p. 127 (2017) [Poster, peer-reviewed].

[9] S. Shimomura, T. Nishimura, Y. Ogura, and J. Tanida, "Optical fabrication of DNA hydrogel using holographic pattern," Information Photonics 2017 (IP'17), IP–21AM–2–2 (2017) [Oral, peer-reviewed].

Others

Publications

[1] M. Nakagawa, Y. Miyata, N. Tate, T. Nishimura, S. Shimomura, S. Shirasaka, J. Tanida, and H. Suzuki, "Spatiotemporal model for FRET networks with multiple donors and acceptors: multicomponent exponential decay derived from the master equation," Journal of the Optical Society of America B, **38**, 294–299 (2021) [Peer-reviewed].

Preface

Complex systems are frequently built from very simple components. Similarly, objects are often regarded as an ensemble of small elements. The function of an object can be realized by cooperative work between its elements. Even if the performance of individual elements is simple, sophisticated actions and unique characteristics can be achieved owing to the capability of the ensemble. An ensemble of elements that are physically and functionally connected to each other is considered as a network.

Nanotechnology has been developed to use the characteristics of nano-objects and to reveal their behaviors. For example, the synthesis of molecules enables the creation of unique material properties such as luminescence emission, which is applied to observing biomolecules. Moreover, the functions of nano-objects can be enhanced by them interacting with each other. A system in which nano-objects communicate with each other via binding and energy can be regarded as a network. The structural change of a nano-object network in response to environmental stimulation can change its physical properties, such that it physically affects an object that is much larger than a nano-object itself. Furthermore, communication in nano-object networks via energy in response to optical signals is useful for computing because it is usually associated with nonlinear processes. Nanoscale information processing systems have actually been established based on the reactions of nano-object networks induced by environmental change. Nano-object networks have a wide range of applications in various fields such as biology and information science.

Self-assembly and the phenomenon of energy transfer are useful for constructing networks. However, self-assembly is based on predetermined chemical reactions that are uncontrollable, whereas energy transfer requires the accurate arrangement of nano-objects. If a network's function can be activated at desired times and spaces, phenomena that exhibit dynamic and spatial changes can be handled. This is useful for analyzing and using the stochastic behavior of objects. To realize the spatial and dynamic activation of a network's function, it is necessary to induce interaction between nano-objects via external stimuli.

Optical control is a promising way of activating the function of nano-object networks owing to its features including spatial parallelism and controllability. Optical methods enable induction of the reaction of nano-objects remotely and dynamically. The use of optical patterns provides parallel processing for nano-objects in the network. The choice of irradiation wavelength also enables nano-objects to be affected selectively. These

capabilities are useful for activating the functions of nano-objects at desired times and spaces, and enable flexible use of nano-object networks.

In this dissertation, a photofunctional nano-object network and its applications are presented. Optical signaling can induce the cooperative work of nano-objects, and enable the function of the network to be activated at desired times and spaces. Flexible activation is helpful to handle dynamic processing on the microscale and nanoscale. To demonstrate the capability of photofunctional nano-object networks, two types of such a network and their applications are investigated. The first is a network using DNA. By a photo-induced reaction, the chemical interaction between DNAs is induced, and the structure of the DNA network can be changed. Physical processing is realized via the change in physical property of DNA networks due to the structural change. The second type is a network using quantum dots (QDs). This is achieved by constructing a networking system with QDs communicating with each other via energy. According to optical signals, the physical interactions between QDs are induced and a network system in which QDs communicate with each other via energy can be constructed. By using the signal modulation depending on the energy state of QDs in the network, information processing is realized. Individual network systems are constructed by optical signals, and the effectiveness of photofunctional nano-object networks is demonstrated.

Chapter 1 presents the concept of a photofunctional nano-object network and fundamental techniques for its realization. Self-assembly and the phenomenon of energy transfer are useful for constructing nano-object networks. In this dissertation, DNA and QDs are focused on as components to construct such networks. Their properties, applications, and current state of research are described. Furthermore, principles and techniques to induce reactions of nano-objects using optical signals are explained. The concept and the potential benefits of photofunctional nano-object networks are also shown. In the last part of this chapter, research topics presented in this dissertation are summarized. The following chapters are divided into two parts to demonstrate the validity of photofunctional nano-object networks. The first part (Chapters 2 and 3) deals with a DNA network and modulation of the mobility of micrometer-sized objects as an application. In these chapters, the function of the network is activated by control of the interaction between the nano-objects (DNA motifs) using photo-induced reactions. The second part (Chapters 4 and 5) deals with a QD network and the possibility of using it for information processing. As described in these chapters, the function is activated by network construction based on photo-induced reactions. Both approaches allow activation of the function of photofunctional nano-object networks dynamically in a spatially controlled manner.

Chapter 2 presents a method for patterning a DNA network using optical signals. DNA plays a key role in storing biological information, and it is a remarkable material to realize nanoscale processing systems through autonomous reactions and molecular modifications. A typical example of a DNA network is a DNA gel. Spatial formation of DNA gels is

equivalent to the creation of regions with high-density DNA and increased viscosity, which enables the motion of an object that is much larger than DNA itself to be affected. By using control of the denaturation of double-stranded DNA by a photothermal conversion effect of quenchers, a method for the optical formation of DNA gels is achieved. Experimental results are shown to demonstrate that DNA reactions are induced in response to optical signals, and patterned DNA gels are formed on the micrometer scale.

Chapter 3 presents the physical processing of a micrometer-sized object using the change of state of a DNA network induced by an optical signal. Optical decomposition of DNA gels enables the viscosity to be decreased spatially and dynamically. The generation of a viscosity gradient results in enhanced mobility of an object. An experimental result is also presented to demonstrate microscale patterning of DNA gels based on optical decomposition. Additionally, the degree of motion of micrometer-sized beads in response to optical signals is shown to verify the effectiveness of this method.

In Chapter 4, a method to generate diverse signals using a QD network constructed by an optical signal is shown. A QD is a nanoparticle converting absorbed energy to fluorescence. Between QDs, energy transfer on the nanoscale arises via optical excitation. By the generation of multistep energy transfers due to the optical excitation of QDs, randomly distributed QDs form a network connected by energy transfers. In this network, the energy state of each QD is modulated dynamically depending on the optical signals, and a variety of temporal and spectral signals can be generated. In the experiment, several types of randomly distributed QD are prepared. A diversity of spectral and temporal signals depending on the irradiation conditions is shown.

In Chapter 5, the possibility of information processing using a QD network is shown. A QD network shows temporal responses modulated by the energy state of QDs depending on the optical inputs. This modulation is a source of dynamics of the fluorescence signal. The dynamics can be used to predict temporal information. To investigate the ability to use this in temporal information processing, a mathematical model of a QD network is constructed. By simulation, fluorescence responses from the randomly distributed QDs according to the optical input are shown. Furthermore, the simulation result on time-series data prediction using a QD network is shown. Finally, the achievements of each chapter are summarized, and the conclusion of this dissertation and a discussion on future issues are presented.

Acknowledgements

Through my Ph. D. program, I has been fortunate to meet mentors, colleagues and friends. First, I would like to express my gratitude to my supervisor in the laboratory of Information Photonics, Dr. Yusuke Ogura in Graduate School of Information Science and Technology, Osaka University, for his kind guidance through intensive discussions and valuable comments. I also would like to express my gratitude to Prof. Jun Tanida in Graduate School of Information Science and Technology, Osaka University, for his guidance and suggestion for five years as a head of the laboratory. I also appreciate my dissertation advisor, Prof. Yasumasa Fujisaki and Prof. Hideyuki Suzuki in Graduate School of Information Science and Technology, Osaka University, for giving effective comments to improve my dissertation. I would like to appreciate Dr. Takahiro Nishimura in Graduate School of Engineering, Osaka University. His suggestion through valuable discussions encouraged me to proceed my research. I also would like to appreciate Dr. Naoya Tate in Graduate School of Information Science and Electrical Engineering, Kyushu University, in for his cooperation to my research. I thank Mis. Makiko Matsushita for her office procedure and kind supports in the laboratory. Moreover, many seniors and juniors in the laboratory supported me. Thank you for their kindness.

I can not imagine life during Ph. D. program without my friends Toshiki Kubo, Kentaro Nishida, Ryo Kato, Ashuya Takemoto, Keigo Nishida and Taiki Matsushita. Especially, I thank Daigo Oue for giving endless discussion about not only our researches but also our future. Their research activities and casual conversions encourage me. Thank you for the friendly competition.

Table of contents

Preface **iii**

Acknowledgements **vii**

1 Introduction: Nano-object network and photoinduced reaction **1**

1.1 Introduction 1

1.2 Nano-objects and their applications 2

1.2.1 DNA 2

1.2.2 Quantum dots 3

1.3 Nano-object network 4

1.3.1 Nano-object network based on chemical reaction 4

1.3.2 Nano-object network based on physical interaction 5

1.3.3 Limitation of nano-object networks 5

1.4 Optically induced reaction of nano-objects 6

1.4.1 Excitation and energy emission of fluorophores 7

1.4.2 Denaturation control of double-stranded DNA based on nonradiative relaxation process of quenchers 7

1.4.3 Multistep FRETs and level occupancy effect 8

1.5 Optical control of nano-object network 9

1.6 Research topics in dissertation 10

2 Optical formation of microscale patterned DNA gels **13**

2.1 Introduction 13

2.2 Reaction scheme 14

2.3 Experiment: Formation of DNA gels by light irradiation 14

2.4 Quantitative evaluation of formed DNA gel for irradiation conditions . . . 17

2.5 Patterning of DNA gel based on photo-induced formation 20

2.6 Discussion 22

2.7 Conclusion 22

3 Optically controlled DNA gel decomposition and modification of object mobility on micrometer scale **23**
3.1 Introduction . . . 23
3.2 Reaction scheme . . . 24
3.3 Decomposition of DNA gels by light irradiation . . . 24
3.4 Patterning of DNA gel based on optical decomposition . . . 27
3.5 Mobility modulation by optical decomposition of DNA gel . . . 31
3.6 Discussion . . . 33
3.7 Conclusion . . . 33

4 Spectro-temporal signal generation using quantum dot network **35**
4.1 Introduction . . . 35
4.2 Signal generation using QD network based on multistep FRET . . . 36
4.3 Spatio-spectral signal variation depending on the irradiation position of aggregated QDs . . . 36
4.4 Temporal signal variation of QD ensemble depending on the irradiation conditions . . . 38
4.4.1 Temporal decay depending on the irradiation intensity . . . 40
4.4.2 Temporal decay depending on irradiation wavelength . . . 42
4.5 Conclusion . . . 43

5 Possibility of temporal information processing using quantum dot network **45**
5.1 Introduction . . . 45
5.2 Mathematical model of a quantum dot network connected by FRETs . . . 46
5.3 Numerical simulation of temporal signals generated from a QD network . . . 47
5.4 Time-series data prediction using temporal signal from QD network . . . 50
5.5 Discussion . . . 54
5.6 Conclusion . . . 54

Conclusion **57**

Appendix **61**

Bibliography **63**

Chapter 1

Introduction: Nano-object network and photoinduced reaction

1.1 Introduction

Construction of a nano-object network in which nano-objects cooperate with each other is an effective way of building a desired physical or information processing system. To construct such a network, it is necessary to design the reaction scheme of nano-objects. However, it is difficult to change the reactions at desired times and spaces because the interactions between the nano-objects are predetermined. To overcome this problem, light can be used to induce reactions via external signals. By using the various interactions between optical signals and nano-objects, the function of a nano-object network can be activated at desired times and spaces. This is useful in handling the dynamic and spatial changes of phenomena on micrometer and nanometer scales.

This chapter presents an overview of photofunctional nano-object networks, aimed at handling the dynamics of micrometer- and nanometer-sized objects. In Section 1.2, the properties of nano-objects are explained. In this research, two types of nano-object are considered and the unique functions of each of them are shown. Section 1.3 describes nano-object networks. Methods to construct such networks and their useful applications are explained. Moreover, problems and limitations of nano-object networks are also presented. Section 1.4 explains optical techniques to control a nano-object. Optical excitation enables the reaction of nano-objects to be induced remotely. The principles of photo-induced reactions and the optical techniques for controlling nano-objects are also presented here. In Section 1.5, features of optically controlled nano-object networks are explained. Section 1.6 describes purpose of this research and research topics for the demonstration.

1.2 Nano-objects and their applications

Nano-objects have various physical and chemical properties and perform functions by interacting with each other. These properties can be applied to a wide range of engineering purposes, including in biology, nanotechnology, and information science. This research focused on two types of nano-object: DNA and quantum dots (QDs). Applications using their properties are also presented.

1.2.1 DNA

DNA is a nano-object with a double-helix structure that plays a key role as a genetic information carrier in biological systems [1]. The genetic information is encoded into sequences of nucleotides consisting of a nucleobase, a sugar, and a phosphoric acid. DNA consists of four kinds of nucleobase: adenine (A), guanine (G), cytosine (C), and thymine (T), as shown in Fig. 1.1. Adenines and guanines bind thymines and cytosines through hydrogen bonds, respectively. Double-stranded DNA (dsDNA) is formed by the combination of nucleobase binding based on Watson - Crick base pairing [2]. The length of one nucleotide along the sequence is 0.30–0.34 nm. A helix cycle consists of 10 base pairs and the helix diameter is 2.0 nm [3, 4]. DNA forms a particularly stable structure, so DNA structures can be designed based on the binding stability obtained from standard enthalpy and standard entropy. These thermodynamic parameters in the formation of dsDNAs can be calculated using, for example, the nearest-neighbor model [5, 6].

By considering the smallest standard Gibbs free energy, the structure of DNA can be predicted. Various software programs [7, 8] to predict DNA structures and design DNA sequences are now publicly available, and desired DNA structures can be easily designed.

A self-assembly of DNA has been used in various fields such as information science and bioengineering. For example, by encoding symbols into DNA sequences, DNA can process mathematical problems [9]. Furthermore, a random search algorithm using self-assembly of DNA was proposed and non-deterministic problems such as Hamiltonian problems [10] and 3SAT problems [11] were solved.

The abilities of DNA can also be extended by modifying it with other functional molecules. For example, the combination of DNA and fluorescence molecules has been used as a probe to detect specific molecules [12]. It has also been described that DNA probes modified with gold nanoparticles or aptamers can report the existence of DNA [13, 14] or RNA [15]. The binding and denaturation processes of DNA also occur stochastically. By using this stochasticity, super-resolution imaging [16] and measurement of pico-Newton cellular traction forces [17] have been achieved.

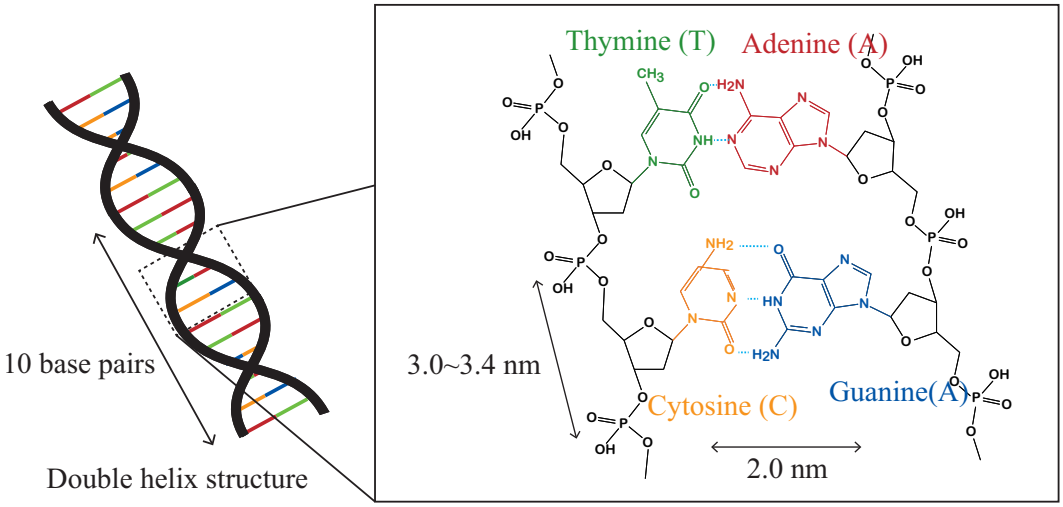

Fig. 1.1 Watson-Crick base pairing and DNA structure

1.2.2 Quantum dots

Quantum dots (QDs) are nanometer-sized particles that generate fluorescence after absorbing light energy. A well-known form is a core/shell-structured QD [Fig. 1.2 (a)]. This QD type consists of a core, made of a semiconductor such as CdSe, and a shell, made of an inorganic material such as ZnS [18]. The core converts light energy to fluorescence, while the shell plays an important role in maintaining the photochemical stability of the core by cloaking. This structure realizes efficient conversion to fluorescent energy, and the quantum yield of the QD has been reported to exceed that of organic fluorophores [19, 20].

QDs have a wide excitation spectrum and absorb light with a wavelength ranging from 300 to 600 nm [21]. The high quantum yield and broad absorption spectrum are useful in solar cells, which convert the energy of sunlight into electric power [22]. The fluorescence spectrum is almost line-symmetric around the peak position of the fluorescence wavelength [18], and FWHM of the spectrum is 30–40 nm, which is narrower than that of an organic fluorophore. Moreover, the peak wavelength of the spectrum depends on the size of the QD, and it can be tuned easily [23]. By attaching molecules to them, QDs can be used in various environments and be applied to biosensing. The high fluorescence intensity of QDs enables the high-contrast observation of single molecules [24] and live cell imaging [25]. Additionally, owing to QDs' photostability, long-term imaging of blood vessels in living mouse was realized [26]. Moreover, QDs can transfer their energy to nearby fluorophores [27, 28]. Indeed, it was reported that the increase of fluorescence intensity due to the energy transfer induced by the aggregation of QDs enables detection of trinitrotoluenes [29] and the binding between an antibody and an antigen [30].

By light irradiation, electrons in QDs are excited and transferred to excitation levels. Then, a hole-electron pair is generated. This excited electron can reduce oxygen. This

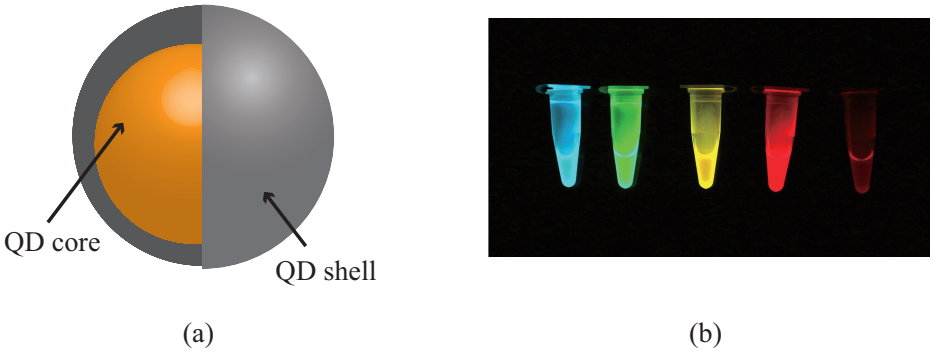

Fig. 1.2 (a) Structure of a core/shell-type QD. (b) QD solutions under UV irradiation.

reduction reaction has been used as a photocatalyst for the degradation of organic pollutants [23]. Furthermore, control of the hole-electron pairs in QDs has been used to provide the emission of laser light [31].

1.3 Nano-object network

A nano-object provides various functions by interacting with each other. This interaction can be regarded as a factor which links nano-objects. When an interaction occurs, the nano-objects bind to each other and transfer energy from nearby nano-objects. As a result, nano-objects can behave in a specific way as a whole system. Such a system that establishes functions which cannot be implemented by a nano-object itself can be regarded as a network consisting of nano-objects. A nano-object network can be constructed by designing a reaction scheme of the nano-objects. At nano-object network based on chemical reaction, the nano-objects are linked via a binding. This network shows remarkable physical properties such as elasticity and viscosity. At nano-object network based on physical reaction, the nano-objects are linked via energy. This network modulates input signals depending on the energy state of nano-objects. This section presents methods for constructing a nano-object network (Fig. 1.3).

1.3.1 Nano-object network based on chemical reaction

The first approach involves designing nano-objects using their chemical reactions. Self-assembly along with the design of DNA sequences is useful for the construction of a network structure via hydrogen bonds. In 1983, N.C. Seeman proposed an artificial connected DNA network structure [32] for the first time. Subsequently, E. Winfree *et al.* succeeded in forming three-dimensional (3D) DNA crystals by designing different reaction schemes for individual DNA strands [33] and demonstrated that DNA has the ability

to construct such a network. In 2006, P. Rothemund formed a complicated DNA network, called DNA origami [34]. Over the past decade, several methods to construct DNA networks have been proposed, and the network size has been scaled up to a few micrometers [35–39]. These networks are useful for establishing DNA nanomachines. It was reported that strand displacement of DNA on a DNA network provided movement of a DNA machine that carried specific molecules [40] and sorted a fluorescent dye [41]. A spring-shaped DNA network also enabled measurement of the mathematical force of myosin [42]. Moreover, by constructing a tubular network structure, the rotational motion of DNA ensembles in response to electronic signals was achieved [43].

DNA networks can also be constructed by using cross-linking reactions of DNA and intermolecular forces. In this method, the network consists of a few types of nano-object [44], and a large-scale structure is realized by self-assembly. Owing to the large scale, the structural change of the DNA network enables a change in its physical properties. A DNA gel, which is a kind of DNA network formed with numerous DNA motifs [45], was reported to be able to transform to the solution state via a change of temperature [46] or pH [47], or by the existence of specific metals [48]. This state transition can be visualized and was shown to be useful for detecting biomolecules such as cocaine [49] and thrombin [50]. Moreover, the mobility of a cell can be regulated by the formation of DNA gels based on the aggregation of DNA motifs [1, 51–53].

1.3.2 Nano-object network based on physical interaction

The second method of constructing nano-object networks involves using physical interaction between nano-objects. The phenomenon of energy transfer based on dipole-dipole and electronic interaction is useful for constructing networks connected via energy. By aligning QDs, it was reported that an energy transmission system on the nanoscale was achieved [27, 54, 55]. Additionally, QDs arranged in a ring were considered to be a networking system, which preserved energy and worked as nanometer-sized memory [56]. Moreover, the structural change of a network was shown to enable modulation of the fluorescence signal from scattered QDs [57]. The phenomenon of energy transfer can also be used for the aggregation of QDs to realize highly efficient modulation of signals [58]. Using the ligands as a scaffold for the network, the QDs can be aggregated and work as a photodiode [59].

1.3.3 Limitation of nano-object networks

By constructing a network, the nano-objects within it can perform diverse functions. To realize each function of a network based on chemical interaction, it is necessary to design the reaction scheme. However, the reaction is predetermined and it is difficult to control the interactions of a nano-object network after its design. Additionally, a problem

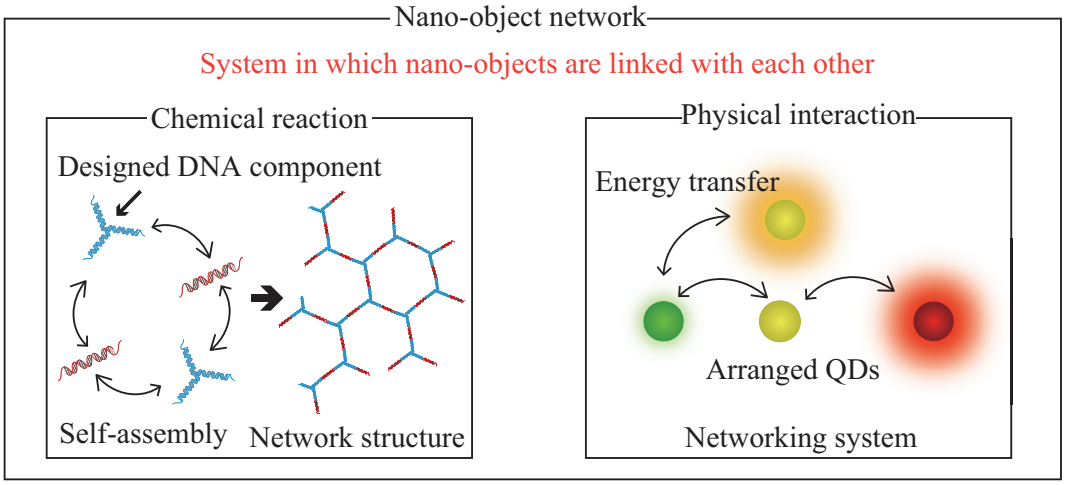

Fig. 1.3 Two types of nano-object network and the mechanism of their construction.

associated with networks based on physical interaction exists. Specifically, to use the energy transfer phenomenon, it is necessary to arrange QDs accurately. However, it is difficult to arrange numerous QDs, and the scalability of the function is poor. A common problem in each network is the lack of control after it has been constructed; specifically, the function cannot be controlled except by designing the network appropriately. However, if the function of a nano-object network is instead activated dynamically in spatially controlled manner, the capability of the network can be extended. Dynamic reaction control of nano-objects enables the stochastic behavior of an object to be handled, which leads to the analysis and utilization of molecular dynamics. Moreover, a spatially induced reaction provides control of the behavior and contributes to manipulation of the object. To achieve this, it is important to induce the reaction of nano-objects in a manner controlled by external signals.

1.4 Optically induced reaction of nano-objects

An optical method is a promising way of inducing reactions of nano-objects. Some nano-objects can be excited by an optical signal and react with each other. A photo-induced reaction is a useful tool to activate the function of a nano-object network dynamically. For example, it was reported that some nano-objects can change their structure and act as nanoscale actuators [60]. Moreover, near-field light generated from a gold nanoparticle was shown to enable observation of aluminum film on the nanoscale [61]. In this section, the mechanism of optical excitation of nano-objects and useful photo-induced reactions to activate the function of nano-object networks are shown.

1.4.1 Excitation and energy emission of fluorophores

Figure 1.4 shows a Jablonski diagram that illustrates the process of excitation and energy emission of fluorophores such as QDs. Electrons in fluorophores transition between two groups of energy levels. By optical excitation, electrons at the ground levels are transferred to one of the excited levels. The excited state of electrons is unstable, and the electrons return to the ground levels by releasing their energy. Such energy is released via two processes: radiative and nonradiative relaxation processes. Through the radiative relaxation process, optical energy is released as fluorescence and phosphorescent. In contrast, through the nonradiative relaxation process, heat and vibration of a fluorophore are generated. The ratio of the energy released via radiative and nonradiative relaxation processes differs depending on the fluorophore. Furthermore, when the excited fluorophore (donor) is near a non-excited fluorophore (acceptor), the energy of the donor is transferred to the acceptor QD. As a result, the excited electron in the acceptor falls to the ground state without emitting energy, and an electron in the acceptor is transferred to the excited levels. This phenomenon is called Förster resonance energy transfer (FRET) [27,62]. FRET efficiency is expressed as follows:

$$E = \frac{R_0^6}{R_0^6 + R^6}. \tag{1.1}$$

R is the distance between a donor and an acceptor. R_0 is Förster distance, which is the distance when FRET efficiency is 50%. R_0 between a donor i and an acceptor j is written as follows:

$$R_0^6(i,j) = \frac{9(\ln 10)\kappa^2 \Phi_{\mathrm{D}}}{128\pi^5 n^4 N_A} \int_0^\infty f_i(\lambda)\varepsilon_j(\lambda)\lambda^4 d\lambda, \tag{1.2}$$

where κ, Φ_D, N_A, $f_D(\lambda)$, and $\varepsilon_A(\lambda)$ are the orientation factors between the donor and the acceptor, quantum yield of the donor, Avogadro's number, donor emission spectrum, and acceptor absorption spectrum, respectively. The FRET efficiency depends on the pairing of fluorophores and their distance from each other. The process of excitation, emission, and transfer can be induced according to optical signals. To activate the function of a nano-object network, the thermal energy obtained via the nonradiative relaxation process and multistep FRETs is used.

1.4.2 Denaturation control of double-stranded DNA based on nonradiative relaxation process of quenchers

A fluorophore with low quantum yield generates substantially more thermal energy than fluorescent energy. This means that heat can be generated in nanoscale by optical excitation. A quencher is a dye molecule with low quantum yield, so it is useful as a heat source [63]. Control of the denaturation of double-stranded DNA (dsDNA) in response to optical signals [64] is achievable by modifying it with quenchers. Figure 1.5 shows a

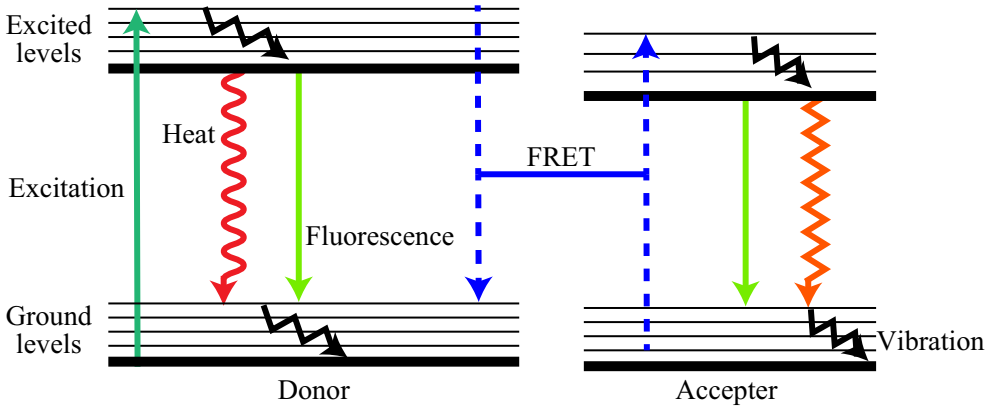

Fig. 1.4 A Jablonski diagram indicating the process of excitation, emission, and transfer of a fluorophore.

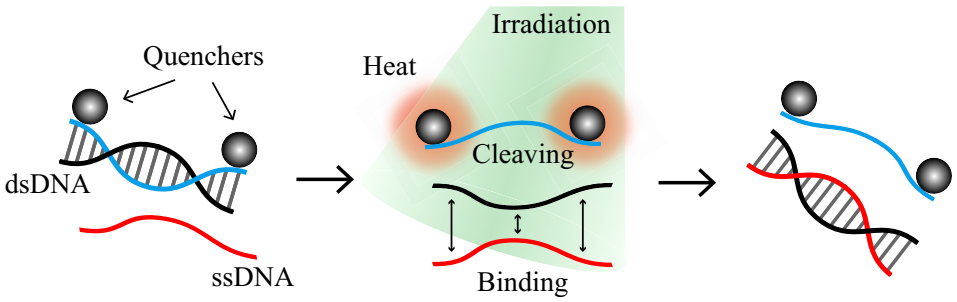

Fig. 1.5 Reaction scheme of DNA strand switching by thermal energy from optically excited quenchers.

reaction scheme of dsDNA denaturation by light irradiation. dsDNA is formed by the hybridization of two single-stranded DNAs (ssDNAs). Quenchers are attached to a strand (blue in Fig. 1.5) of the dsDNA. When the quenchers are excited by light irradiation, thermal energy is generated and the local temperature increases. Because denaturation of the dsDNA is induced at the produced high temperature, the dsDNA separates into two strands: blue and black strands shown in Fig. 1.5. The red ssDNA is complementary to the cleaved black ssDNA, and they begin to bind. Consequently, binding exchange of ssDNA can be induced by light irradiation.

1.4.3 Multistep FRETs and level occupancy effect

A QD transfers excitation energy to a neighboring QD by FRET. When multiple QDs are present, the energy of the excited QDs is transferred one after another by FRETs [Fig. 1.6 (a)]. By distributing QDs for inducing multistep FRET, a multistep energy transmission

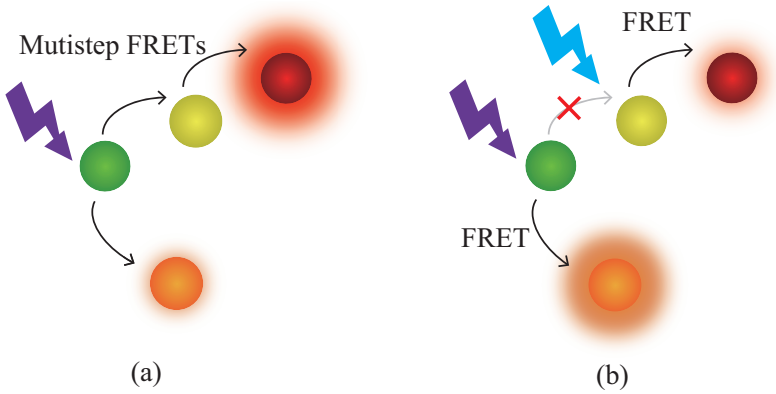

Fig. 1.6 (a) Multiple FRET generation. (b) Change of FRET pathway by optical excitation of relay nano-object.

system can be realized [55, 65, 66]. Moreover, multiple FRETs can be inactivated by optical excitation of the relay QDs. In the excited acceptor, many electrons are at the excited levels. The acceptor dissipates the energy and refuses to receive additional transferred energy [31,67–69]. As a result, the FRET pathways are changed depending on the irradiation conditions. This is called the level occupancy effect. When multiple QDs are located and excited simultaneously by the light, as shown in Fig. 1.6 (b), the FRET pathway is changed depending on the individual QDs' energy state, and the fluorescence signal is correspondingly generated. By using this phenomenon, signal modulation depending on optical signals can be achieved [69, 70].

1.5 Optical control of nano-object network

Optical control enables the dynamic actuation of nano-objects by introducing a photo-induced reaction, by which physical and information processing can be realized. In previous studies, DNA nanomachines modified with photoisomerized molecules and fluorescent material were activated by light irradiation [71,72]. The signal modulation of excited QDs based on FRET was reported to achieve the detection of molecules [27, 28]. These examples suggest that the use of optical signals is effective to achieve dynamic control of the function of nano-object networks. From the perspective of optical control, a nano-object network can perform useful functions. The dynamic control of a nano-object network enables activation of its function at desired times and spaces and appropriate handling of the dynamics of an object. Furthermore, the use of light also contributes to simplifying the design of nano-object networks. The construction of such networks requires the accurate arrangement of nano-objects to activate the function by a predetermined reaction [73, 74]. In the optical method, the function can be induced from the external en-

vironment, making it unnecessary to design an elaborate reaction scheme. Moreover, the use of a nano-object network enables the capability of optical methods to be expanded. The operation scale of the optical control should be greater than several hundred nanometers due to the diffraction limit. In contrast, a nano-object network can work in a wide range of sizes from nanoscale to millimeter scale, and optical operation for a wide range of objects can be realized. A combination of optical control and a nano-object network thus enables physical or information processing on various scales.

1.6 Research topics in dissertation

This dissertation presents a new approach to expand the functionality of nano-object networks by using optical techniques. The interaction to construct nano-object network is generally classified into two type: chemical and physical interaction. In the research, two types of nano-object are used to demonstrate the capability of individual nano-object networks.

Figure 1.7 shows the structure of this dissertation. This dissertation consists of two parts. The first part deals with a DNA network and its application to modulate the mobility of a micrometer-sized object. A typical example of DNA networks is DNA gels. DNA gels are formed by constructing a network structure using chemical interactions and have high viscosity. In this research topic, the function of DNA gels is activated by controlling the chemical reaction of DNA using the nonradiative relaxation process of excited quenchers. The second part deals with a QD network and its potential use for temporal information processing. In this case, by the irradiation of optical signals, physical interactions via energy are generated between QDs. Energy transfers according to the optical input modulate the energy state of QDs, and variation of the temporal and spectral signals from the QDs is generated. This system in which QDs communicate with each other via energy given by optical input can be regarded as a networking system consisting of QDs. In this research topic, by inducing multistep FRET in randomly distributed QDs according to the optical signals, the QD network is constructed and signal dynamics that are essential for processing temporal signals are created. Both approaches enable activation of the function of the network at the desired time and space. The details of the content described in each chapter are as follows.

1. Optical formation of microscale patterned DNA gels (Chapter 2)

A change of state of a nano-object network enables modulation of its physical properties. This change of properties can affect objects that are much larger than nano-objects themselves. The spatial formation of a DNA network enables the motion of the object

to be affected. In this topic, the optical patterning of a microscale DNA gel, which is a DNA network constructed by self-assembly, is presented. Using thermal energy via a non-radiative relaxation process of excited quenchers, the DNA gels are formed in response to optical signals. In the experiment, the microscale patterning of DNA gels by patterned light irradiation is shown. These results are based on a previous study [75].

2. Optically controlled DNA gel decomposition and modification of object mobility on micrometer scale (Chapter 3)

The change of spatial state of a DNA network creates a viscosity gradient and implements physical processing of the object's mobility. This topic presents a method to decompose DNA gels by light irradiation and to modulate the mobility of a micrometer-sized object based on a decrease in viscosity. In the experiment, the decomposition of DNA gels in response to irradiation patterns on the micrometer scale is shown. Furthermore, modulating the mobility of micrometer-sized beads as a result of decomposition in response to irradiation is confirmed. These results are based on a previous study [76].

3. Spectro-temporal signal generation using quantum dot network (Chapter 4)

The construction of a nano-object network based on physical interaction requires a complicated procedure for accurately arranging its elements. Optical methods provide excitation to the specific elements and induce physical interactions depending on the irradiation conditions. This topic presents an optical method for generating diverse temporal and spectral signals using a QD network connected by FRET. On the basis of the multistep FRETs and the energy occupancy effect, the dynamic modulation of the QDs' energy state is provided, and a variety of fluorescent signals are created from the randomly distributed QDs. In the experiment, the spectral signals of a QD aggregation within different irradiation areas and the temporal signals of a QD ensemble depending on the irradiation conditions are investigated. The results are based on a previous study [77].

4. Possibility of temporal information processing using quantum dot network (Chapter 5)

The diversity of temporal signals generated from a QD network depending on the irradiation conditions is useful for temporal data prediction. The possibility of temporal information processing by using signal modulation of a QD network is shown. To investigate the potential of the QD network, a mathematical model of the QD network is constructed. The simulation result of temporal data prediction using the QD networks is described.

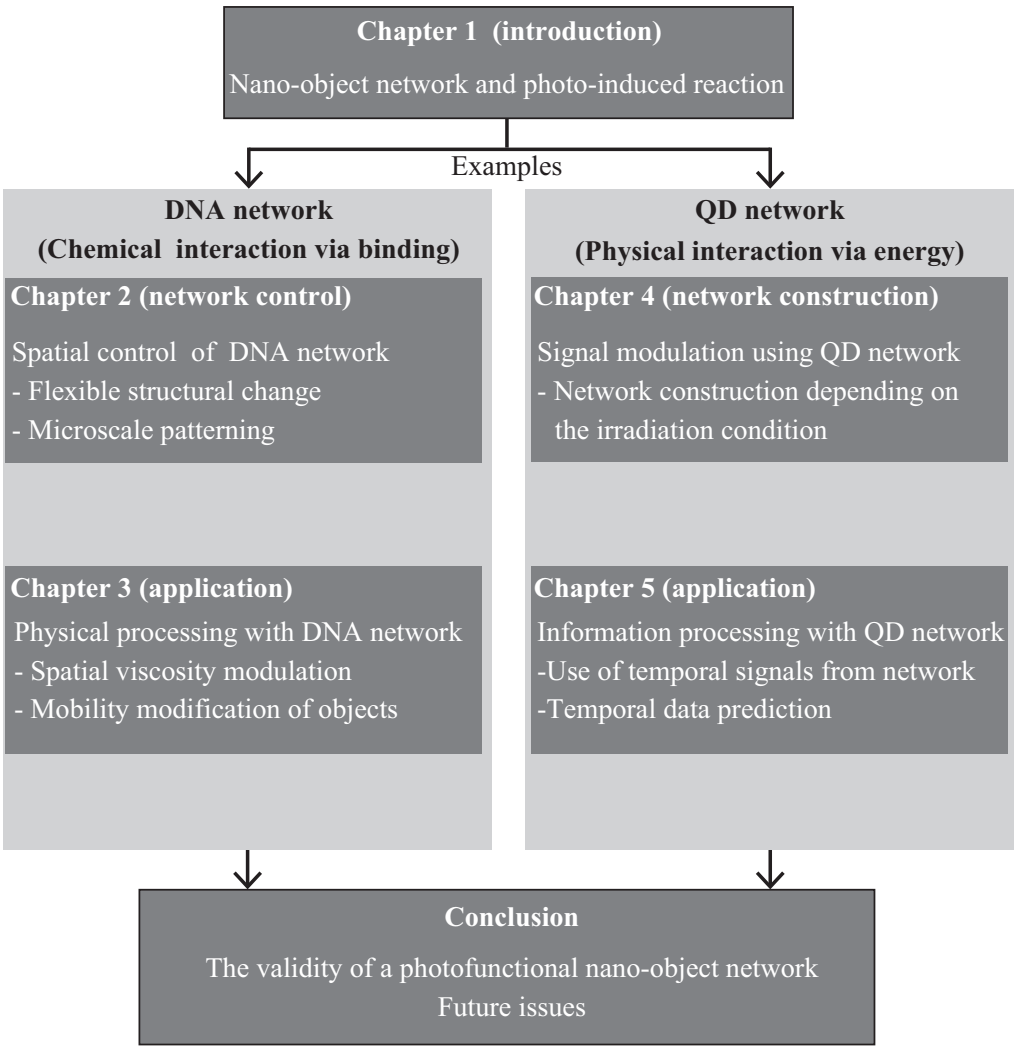

Fig. 1.7 Structure of the dissertation.

Chapter 2

Optical formation of microscale patterned DNA gels

2.1 Introduction

The property of a nano-object ensemble is determined by the structure constructed by nano-objects. The structural change of a nano-object network modulates its physical properties. This change of properties, such as elasticity and water content, enables an object that is much larger than the nano-objects themselves to be affected by them. A DNA gel, which is a DNA network structure constructed by the crosslinking of DNA motifs [44], can be transformed into gel and sol states by the reaction of designed DNA motifs. Pattern formation of DNA gels enables the motion of an object to be affected and is useful for arrangement and manipulation. However, the patterning of DNA gels is implemented using self-assembly induced by an environmental change, and thus it is difficult to form a specific morphology of DNA gels in a flexible manner. To control the shape of DNA gels, the use of a mold with the corresponding shape is a promising method [78]. However, to change the shape, a new mold is required. Another possible method is to induce a DNA reaction spatially, and ink-jet nozzles [51] or substrates coated with DNA initiators [1] are often employed for this purpose. Although these methods can make DNA gels with complicated shapes, it takes a long time to form the desired shape, given the slow scanning of the nozzles or need for coating of DNA on a glass slide.

In this chapter, a method of forming DNA gels by optical control is presented. The use of light enables the induction of DNA reactions at desired times and positions, allowing flexible patterning of DNA gels. In a previous study, formation of a DNA gel was demonstrated using photo-responsive cross-linkers, which are responsive to UV light [79]. However, this method requires accurate temperature control, which makes it difficult to form DNA gels in a spatially controlled and rapid manner. In the proposed method, a DNA reaction scheme using the thermal energy of optically excited quenchers is designed for the optical formation of DNA gels. To demonstrate flexible control over the

DNA gels' shape, light patterns created by computer-generated holograms (CGHs) are employed. Section 2.2 shows a scheme designed to form DNA gels in response to an optical signal. Section 2.3 describes an experimental result on forming DNA gels by light irradiation. In Section 2.4, the relationship between the formation of DNA gels and the irradiation condition are shown. Section 2.5 shows patterned formation of DNA gels corresponding a light pattern. Section 2.6 describes a discussion about the validity and the performance of the method.

2.2 Reaction scheme

Figure 2.1 shows a schematic diagram of the optically-induced formation of a DNA gel. The DNA gel is formed by construction of network structure using Y-motif (Y-DNA) and Linker DNA (L-DNA). The Y-DNAs and the L-DNAs consist of three and two kinds of single-strand ssDNAs, respectively (Y-DNA: Y1, Y2, and Y3, L-DNA: L1, L2). Y-DNA segments are connected to each other through the intermediation of L-DNA segments because they have complementary pairs of sequences at their sticky ends. In the initial conformation, the sticky ends of Y-DNA bind with ssDNAs named Capping DNAs (C-DNAs), which prevents L-DNAs from binding Y-DNAs. C-DNAs are modified with quenchers at both sticky ends to control by light. When the C-DNAs is irradiated with excitation light of a quencher, thermal energy is generated from the quencher [63]. This energy is high enough to cleave the hydrogen bonds between sticky ends of the Y-DNA and of the C-DNAs, and thus, the C-DNAs are denaturated from the Y-DNAs. The cleaved Y-DNAs begin to bind with the L-DNAs to form DNA gels. This process is induced within the irradiated region of the excitation light, and the DNA gel is formed depending on the light intensity distribution. Consequently, the shape can be flexibly controlled by changing the irradiation pattern.

2.3 Experiment: Formation of DNA gels by light irradiation

The scheme was tested by the experiment. First, the formation of each DNA motif used was investigated by agarose gel electrophoresis. To confirm that each DNA strand binds with each other and forms the Y-DNA and the L-DNA, eleven samples were prepared. Table 2.1 shows the sequence of the DNA strands and the modifications to form DNA gels. In the method, Black Hole Quencher-1 (BHQ-1, peak excitation wavelength: 534 nm) was employed because its photothermal conversion efficiency is high owing to low quantum yield and short fluorescence lifetime [63]. The DNA strands were purchased from Tsukuba Oligo Service C. Ltd. The buffer composed of H_3PO_4(concentration: 74

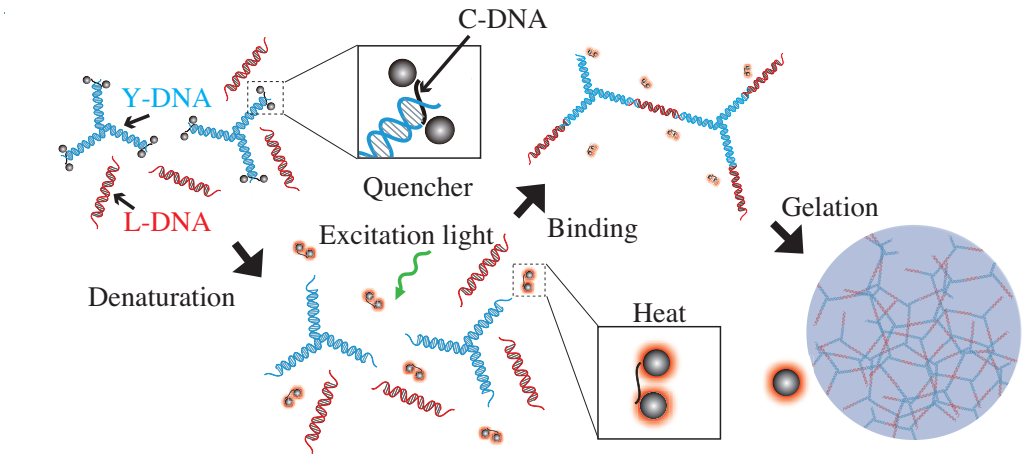

Fig. 2.1 Schematic diagram of DNA gels' formation by light induction

mM) and NaCl (concentration: 240 mM) was prepared, and individual DNA strands were mixed so that the DNA concentration was 5.0 μM. Each sample was added to wells in the agarose gel with mass concentration of 6.0 wt%, and a voltage of 120 V was applied to the gel for 30 min. The electrophoresis image is shown in Fig. 2.2. In the lanes 1-7, the migration distance becomes shorter as the number of DNA strands to form the Y-DNA increases. Moreover, the lane 8 shows the existence of longer DNA strands compared to the lane 7. The result shows that the Y-DNA was formed and bound with the C-DNAs. Similarly, the migration distance of lane 11 is the shortest among lanes 9-11. The result confirmed formation of the L-DNA as expected.

Next, the formation of DNA gel was verified by light irradiation. Two sample tubes containing all DNA motifs (Y-DNA : 6.7 μM, L-DNA: 6.7 μM, C-DNA: 26.8 μM) in the buffer (H_3PO_4: 64.8 mM and NaCl: 210 mM) were prepared. One of the sample was irradiated using a diode-pumped solid state (DPSS) laser (Spectra-Physics KK., Excelsior

Table 2.1 DNA sequences and modifications to form Y-DNA and L-DNA.

Strand name	Sequence
Y1	5'-CGATTGACCACGCTGTCCTAACCATGACCGTCGAAG-3'
Y2	5'-CGATTGACCTTCGACGGTCATGTACTAGATCAGAGG-3'
Y3	5'-CGATTGACCCTCTGATCTAGTAGTTAGGACAGCGTG-3'
L1	5'-GTCAATCGTCTATTCGCATGAGGATCCCATTCACCGTAAG-3'
L2	5'-GTCAATCGCTTACGGTGAATGGGATCCTCATGCGAATAGA-3'
C-DNA	5'-(BHQ-1)-GTCAATCG-(BHQ-1)-3'

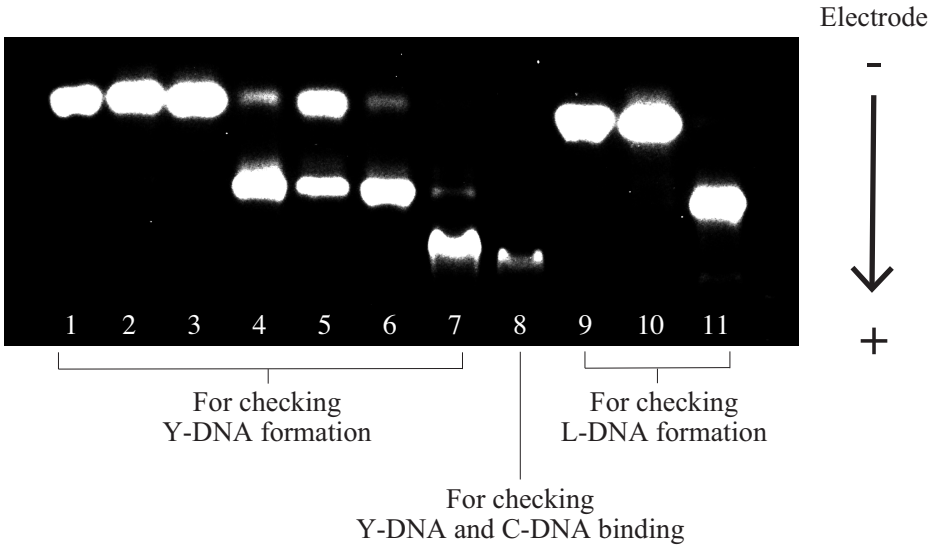

Fig. 2.2 Agarose gel electrophoresis result of samples containing DNA motifs. (1) Y1, (2) Y2, (3) Y3, (4) Y1+Y2 (molar ratio: 1: 1), (5) Y2+Y3 (1: 1), (6) Y1+Y3 (1: 1), (7) Y-DNA (Y1: Y2 : Y3 = 1: 1: 1), (8) Y-DNA+C-DNA (molar ratio = 1: 4), (9) L1, (10) L2, (11) L1+L2 (1: 1).

532 Single Mode, emission wavelength: 532 nm, power: 74.0 mW) at 2.3 W/cm^2. On the other hand, the other sample was not irradiated. After 1 hour, each sample was stained with SYBR green I (peak emission wavelength: 521 nm) and was observed under UV light irradiation using a transilluminator (FUNAKOSHI, NTM-10). SYBR green I generates fluorescence by intercalation in double-stranded DNA; hence, high fluorescence intensity indicates a high dense DNA area. DNA gels have higher DNA density than the DNA solution, and therefore, an area of high fluorescence intensity can be considered as DNA gels. The captured images of non-irradiated and irradiated sample tubes under UV irradiation are shown in Fig. 2.3 (a, b). For the non-irradiated sample, the uniform fluorescence intensity was observed in the entire area. On the other hand, the irradiated sample shows high fluorescence intensity in the bottom area. For further investigation, each sample was dropped on a slide glass and observed with a fluorescence microscope (objective lens: 10×, camera: Basler, acA1920-25um). Figure.2.3 (c, d) show the fluorescence images of individual samples. In the non-irradiated sample [Fig. 2.3 (c)], the fluorescence intensity was entirely uniform. In contrast, high fluorescence areas was observed in the irradiated sample [Fig. 2.3 (d)]. The experimental results show that DNA gel was formed by light irradiation. Furthermore, such formation was not observed in the DNA solutions without L-DNA or Y-DNA. In the scheme, all the components were required to create the DNA gels.

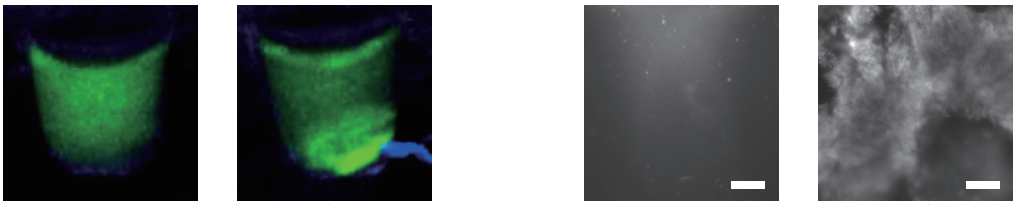

Fig. 2.3 Captured images of (a) non-irradiated and (b) irradiated sample tubes under UV light irradiation. Fluorescence images of (c) non-irradiated and (d) irradiated samples captured using a fluorescence microscope. scale bars indicate 300 μm.

2.4 Quantitative evaluation of formed DNA gel for irradiation conditions

To show an advantage of the optical method, local formation of DNA gels by light irradiation was verified. Figure 2.4 shows the optical setup to observe the local formation of DNA gel under the light irradiation. The light emitted from the DPSS laser passed through the relay lens and is focused on the sample plane using the objective lens (Olympys, UMPlanFI 10×). The fluorescence generated from the sample is observed using a charge coupled device (CCD) image sensor (Roper Scientific, CoolSNAP fx Monochrome) mounted on a fluorescence microscope (Olympus, BX51WI). The sample was composed of each DNA motif (Y-DNA: 15.0 μM, L-DNA: 13.3 μM and C-DNA: 60.0 μM) in the buffer (H_3PO_4: 3.1 mM, NaCl: 8.5 mM). The DNA solution was stained with a DAPI (Dojin, peak excitation wavelength: 360 nm, peak emission wavelength: 460 nm) to observe the formation of DNA gels under the light irradiation. In the experiment, two band-pass filters (transmission wavelength: 330–385 nm for excitation and 475–495 nm for detection) and a dichroic mirror (transmission wavelength: 500- nm) were utilized to excite the DAPI using a white light source and to detect only fluorescence signals.

Figures 2.5 (a) shows time-sequence fluorescence images under irradiation of a single focused laser beam. The irradiation area (diameter: 20.8 μm) is indicated by a circle. The fluorescence intensity becomes higher around the center of the beam as irradiation time increased [Fig. 2.5 (a)]. This shows that the DNA gels formed a circular shape, corresponding to the shape of the light spot. To evaluate the formation of DNA gels depending on light intensity and irradiation time, the diameter of the circular-shaped DNA gels was measured. Using the Hough transformation, the diameter of a high fluorescence intensity area was obtained. The relationship between the irradiation time and the diameters of the DNA gels at individual irradiation intensities (5.4×10^2, 1.1×10^3, 1.6×10^3, 2.1×10^3, and 2.7×10^3 W/cm^2) is shown in Fig. 2.5 (b). The diameters increased as the irradiation

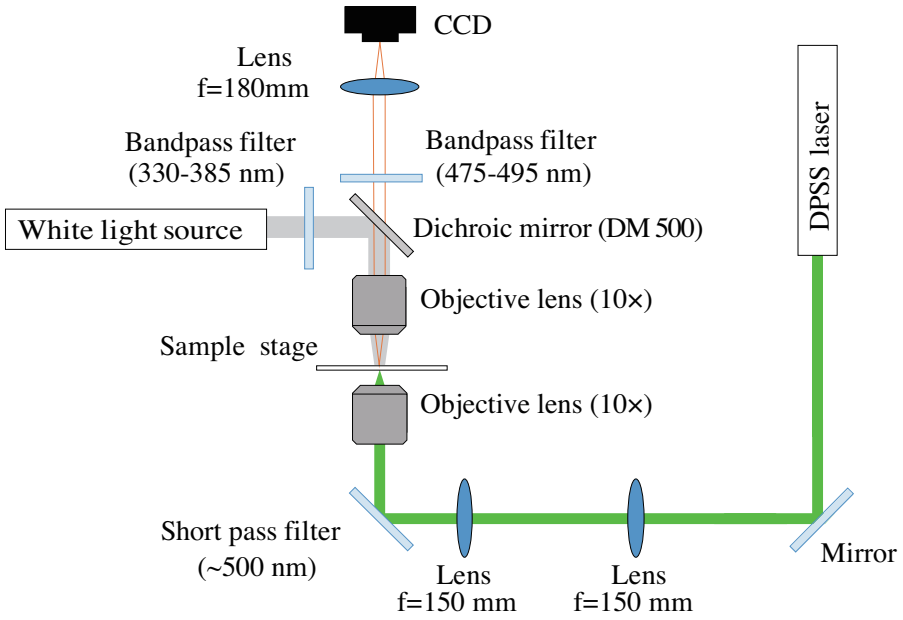

Fig. 2.4 Optical setup to evaluate the formation of DNA gels depending on the light intensity

intensities increased, which shows that amount of the DNA gels increased depending on the light intensity and irradiation time. Moreover, the increasing rate of the diameter gradually decreased as the irradiation time became longer. This result indicates that the amount of formed DNA gels can be controlled depending on the irradiation intensity. However, using the intensity higher than 2.1×10^3 W/cm^2, donuts-shaped DNA gels were formed as shown in Fig. 2.5 (c). A possible reason is as follows. When the sample is irradiated with the excitation light, thermal energy is generated from the quenchers on the C-DNAs. When thermal energy is too much, the hydrogen bonds in Y-DNAs and L-DNAs are cleaved, and the DNA strands are dispersed out of the irradiation area. Thus, within the center area of the irradiation with high intensity, the DNA gels are cleaved contrary to the reaction scheme. To avoid such unexpected structure, it is important to adjust the irradiation intensity less than 2.1×10^3 W/cm^2.

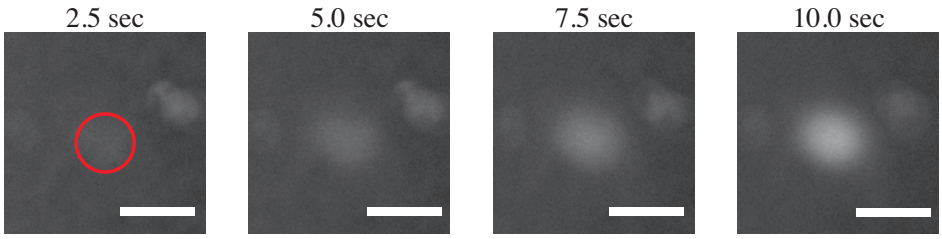

(a)

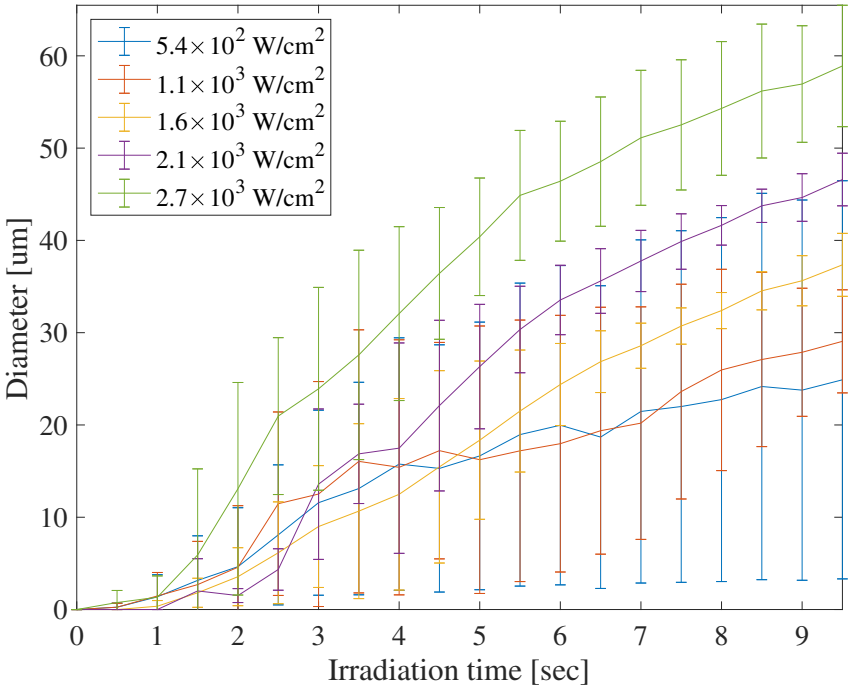

(b)

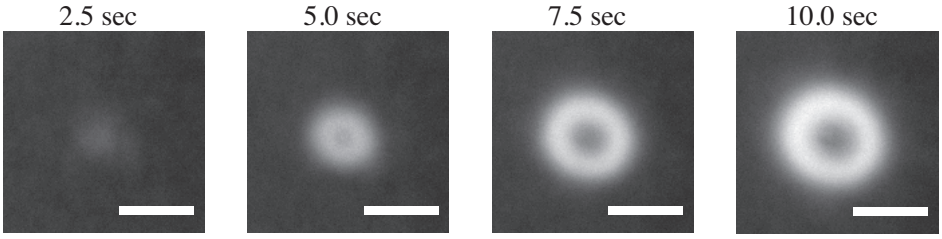

(c)

Fig. 2.5 (a) Fluorescence images obtained under focused light irradiation with 1.6×10^3 W/cm^2. The irradiation area is indicated by a red circle. (b) Relationship between the irradiation time and the diameter of the circular-shaped DNA gels. (c) Fluorescence images taken under the irradiation with 2.7×10^3 W/cm^2. Scale bars shown in (a,c) indicate 30μm.

2.5 Patterning of DNA gel based on photo-induced formation

To demonstrate the spatial controllability of the formation of DNA gels by optical control, the formation of DNA gels using light patterns generated by a spatial light modulator (SLM) was investigated. The optical set-up to generate the light patterns is shown in Fig. 2.6. The beam hits a liquid crystal on silicon-based transmissive SLM (HOLO EYE photonic AG., LC2012, number of pixels:1024×768, pixel pitch: 36.0 μm). The phase modulation patterns displayed on the SLM were designed by using the Gerchberg-Saxton algorithm, so that a desired light pattern was generated on the sample plane [80]. Figure 2.7 (a-e) shows the light patterns at the sample plane. To consider the thermal dispersion of the DNA gels induced by excited quenchers, spot-array patterns were produced. The average intensities of the spots (diameter: 5.0 μm) in the generated patterns shown were 3.8×10^2, 5.1×10^3, 4.9×10^3, 5.0×10^3, and 5.6×10^3 W/cm^2, respectively. The concentrations of individual DNA motifs (Y-DNA, L-DNA, and C-DNA) in the buffer solution (1.3 mM H_3PO_3 and 5 mM NaCl) were 22.2, 22.2, and 88.8 μM, respectively.

Figure 2.7 (f-j) shows the fluorescence images under individual irradiation patterns shown in Fig. 2.7 (a-e). Each fluorescence intensity locally increased corresponding to the individual irradiation patterns. The two-dimensional shape of DNA gels can be controlled by the light pattern irradiation. The overall size of the DNA gels was 70 μm, which demonstrated the ability to form microscale DNA gels. To investigate the shaping resolution in the proposed method, the widths of the formed DNA gels along red lines (see Fig. 2.7 (f-j)) were measured. The width of a DNA gel is defined as that of a region whose intensity is higher than the average fluorescence intensity of the captured image. The widths were (f) 12.1, (g) 14.7, (h) 5.8, (i) 5.8, and (j) 12.7 μm. Differences in the fluorescence intensity were observed in these DNA gels. This may have been due to the fact that the light intensity of each spot in the light pattern varied depending on the irradiation position and the number of spots. To reduce the variation in the spatial formation of DNA gels, it is necessary to adjust the irradiation time and the irradiation pattern.

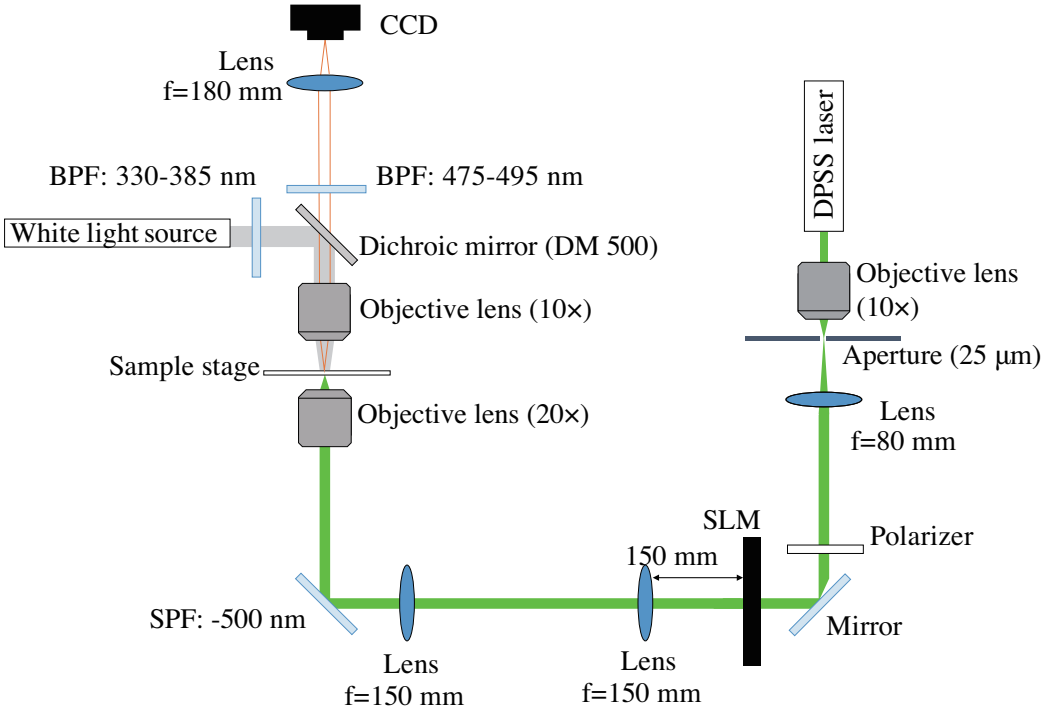

Fig. 2.6 Optical set-up to control DNA gels' shape by light pattern.

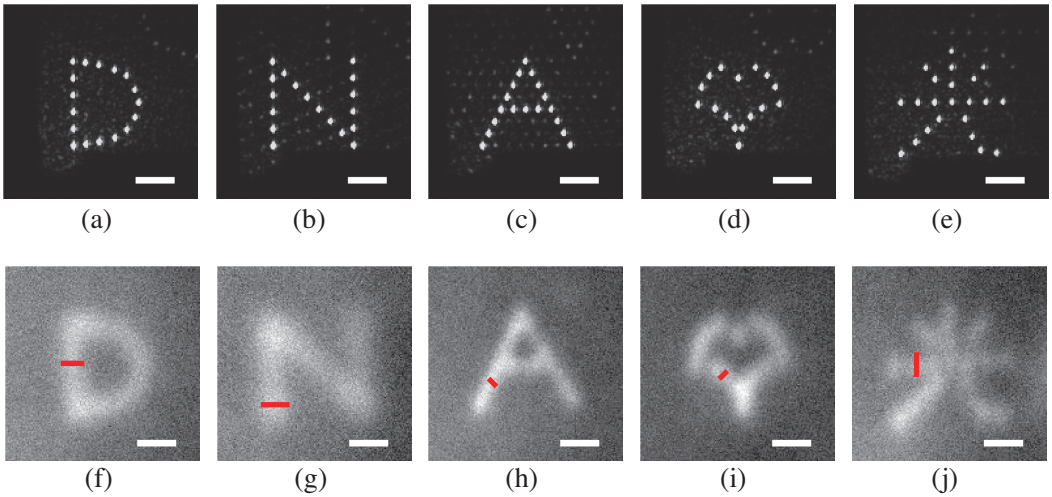

Fig. 2.7 Generated light patterns of (a) D, (b) N, (c) A, (d) ginkgo leaf shape, and (e) a Chinese character that means light. (f-j) Fluorescence images after irradiation for 2.5 s under the irradiation patterns shown in (a-e). Scale bars indicate 20 μm.

2.6 Discussion

To date, the patterning size of DNA gels has been on the order of millimeters [1, 51]. In contrast, as the experiments in this study demonstrated, the optical patterning of DNA gels enabled the fabrication of DNA gels with an overall size of a few hundred micrometers. Therefore, this method enables the handling of micrometer-scale processing, such as regulating the motion of a micrometer-sized object. The size of the light spot can be reduced to a few hundred nanometers, and the DNA gels can be miniaturized to submicron scale. The optical formation of DNA gels with a wide range of sizes enables the handling of objects with a size in the range from submicrons to millimeters. The proposed method also enables the fabrication of 3D DNA gels owing to its spatial controllability. For the formation of 3D DNA gels, it is necessary to stack two-dimensional DNA gels [51]. This stacking is time-consuming because the structure needs to be formed in the correct order from the bottom. The use of a light pattern enables the implementation of parallel processing within the irradiation area without scanning, and also makes the rapid formation of DNA gels with a 3D structure achievable.

2.7 Conclusion

In this chapter, a method for the optical formation of DNA gels is presented as an example of a photofunctional nano-object network. Using control of the denaturation of dsDNA by thermal energy generated from excited quenchers, the formation of DNA gels by light irradiation was achieved. In the experiment, the DNA gels were formed depending on the irradiation area, time, and intensity. Furthermore, using light irradiation with an intensity greater than 2.1×10^3 W/cm^3, donut-shaped DNA gels were formed regardless of the irradiation area. Finally, the DNA gels at a size of 70 μm were appropriately shaped by light patterns. This method enables the formation of DNA gels spatially and dynamically, and can be applied to fabricate a cell scaffold for complicated cell patterns.

Chapter 3

Optically controlled DNA gel decomposition and modification of object mobility on micrometer scale

3.1 Introduction

A DNA gel exhibits high viscosity via the self-assembly of numerous DNAs, and thus can be used to restrict the mobility of objects. This property has been used to trap micrometer-scale objects [52, 53]. However, these trapping techniques are based on chemical reactions between DNA and objects, so it is difficult to control the mobility of objects dynamically. Moreover, objects that do not react with DNA cannot be handled. The dynamic and spatial control of the viscosity of DNA gels would provide a method for flexibly modifying an object's mobility. In Chapter 2, the microscale patterning of DNA gels by optical control was demonstrated. This means that the viscosity increases on the microscale at the desired time and space, and the mobility of a micrometer-sized object can be restricted selectively. If a method for enhancing objects' mobility is realized, the motion of micrometer-sized objects can be controlled according to the change in viscosity of DNA gels. To realize this, it is necessary to reduce the viscosity of a DNA gel via an optical signal that differs from the signal for DNA gel formation to modulate the motion of the object. Optical decomposition of DNA gels using thermal energy generated from excited quenchers provides spatial reduction of the viscosity on the microscale and the dynamic enhancement of an object's mobility. Furthermore, it is possible to combine this with the method for the optical formation of DNA gels because the use of different types of quencher enables induction of the denaturation of dsDNA at different irradiation wavelengths. The selective excitation of quenchers enables control of the viscosity of DNA gels in a reversible manner, and the manipulation of micrometer-sized objects can be achieved by combining with the formation method shown in Chapter 2.

In this chapter, the ability to perform physical processing by using the change of state

of a DNA network induced by optical signals is shown. As a demonstration of this, a method to modulate the mobility of an object on the micrometer scale by the optical decomposition of DNA gels is presented. Section 3.2 explains the reaction scheme for modulation of object's mobility by decreasing viscosity of DNA gels based on optical decomposition. Section 3.3 shows the decomposition of DNA gels by light irradiation. Section 3.4 describes the patterning of DNA gels based on the optical decomposition. Section 3.5 describes viscosity decrease by optical decomposition of the DNA gels and mobility modulation of micrometer-sized objects.

3.2 Reaction scheme

Figure 3.1 shows a schematic diagram of mobility modification as a result of optical decomposition of DNA gels. The DNA gel consists of Y-DNA and L'-DNA. For optical decomposition, the sticky ends of the L'-DNA are modified with quenchers. In the initial state, the DNA gel encapsulate micrometer-sized objects and restrict their mobility. Optical excitation causes quenchers to generate thermal energy through a non-radiative relaxation process. Thus, the bonds between the Y-DNA and the L'-DNA in the DNA gel are cleaved by light excitation, and the DNA gel within the irradiation area is decomposed. The viscosity then decreases owing to the state change of the DNA gel, and the mobility of the micrometer-sized objects is enhanced. After the irradiation, the cleaved sticky ends of Y-DNA bind to ssDNAs (C'-DNAs) that prevents rebinding with L'-DNA due to the presence of a large amount of the C'-DNAs. As a result, the DNA solution maintains its state and viscosity even after the irradiation is stopped. The decomposition ratio depends on the light intensity. Therefore, the viscosity distribution of DNA gels changes depending on the spatial light distribution, and the object's mobility can be modulated dynamically. The designed DNA components are listed in Table 3.1. All DNA strands were purchased from Tsukuba Oligo Service Co. Ltd. The Y-DNA and the L'-'DNA consisted of three (Y1, Y2, Y3) and two (L'1, L'2) kinds of DNA strands, respectively. The 5'- end of L'1 and of L'2 was modified with BlackBerry Quencher 650 (BBQ-650), which is a quencher absorbing light in the wavelength range of 550–750 nm.

3.3 Decomposition of DNA gels by light irradiation

First, DNA solutions containing all DNA motifs were prepared and observed using a fluorescence microscope to confirm decomposition of the DNA gels by light irradiation. Figure 3.2 shows the procedure to prepare samples. The concentration of DNA motifs (Y-DNA, L'-DNA and the C'-DNA) in buffer (H_3PO_4: 2.2 mM, NaCl: 7.1 mM) was 28.6, 28.6 and 228.8 μM, respectively. To form enough amount of DNA gels, the Y-DNAs and L'-DNAs were mixed at first. After keeping test tubes at 6 °C for 3 hours using a

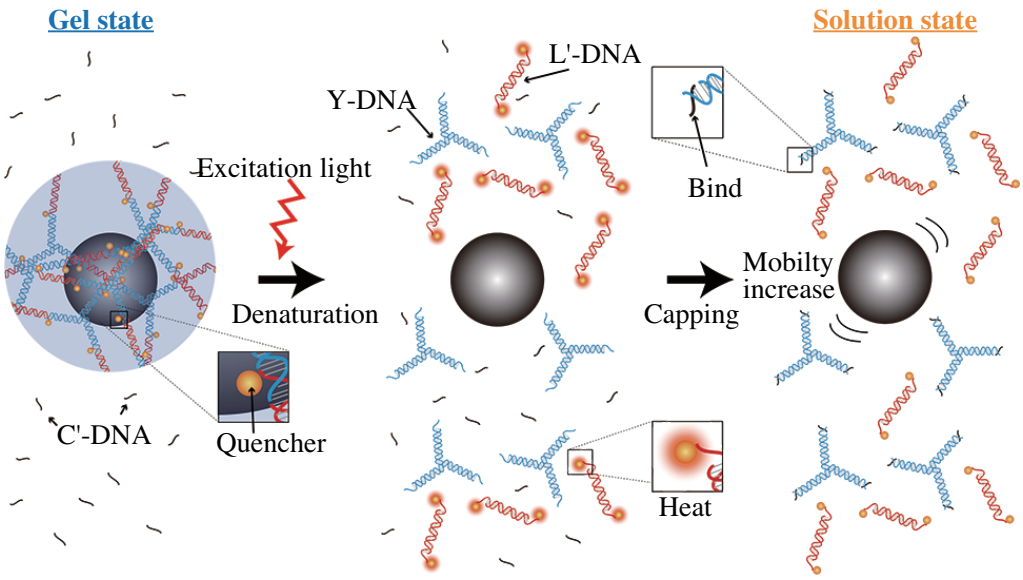

Fig. 3.1 Schematic diagram of mobility modulation by viscosity decrease based on photo-induced decomposition of DNA gels.

thermal controller (ThermoStat plus, eppendorf), the C'-DNAs and DAPI were added to the individual tubes. Figure 3.3 (a) shows a fluorescence image of the samples at the initial state. High florescence intensity is observed in some local areas; this indicates the formation of DNA gels. In addition, one test tube was irradiated with the laser beam (wavelength: 660 nm, intensity: $3.0 \times 10^{-1}\mathrm{W/cm^2}$) emitted from a laser diode (ML101J27, Mitsubishi Electric) for 1 hour. After that, each sample was dropped on a slide glass and observed using a CCD (Roper Scientific, CoolSNAP fx Monochrome).

The fluorescence images of the DNA solution without and with irradiation are shown in Figs. 3.3 (b, c). Compared to the non-irradiated DNA solution [Fig. 3.3 (b)], the uniform fluorescence intensity is observed when the DNA solution is irradiated [Fig. 3.3 (c)]. The result shows the decomposition of the DNA gels by the light irradiation.

Table 3.1 DNA sequences and modifications to form optically-decomposed DNA gels.

Strand name	Sequence
Y1	5'-CGATTGACCACGCTGTCCTAACCATGACCGTCGAAG-3'
Y2	5'-CGATTGACCTTCGACGGTCATGTACTAGATCAGAGG-3'
Y3	5'-CGATTGACCCTCTGATCTAGTAGTTAGGACAGCGTG-3'
L'1	5'-(BBQ-650)-GTCAATCGTCTATTCGCATGAGGATCCCATTC--ACCGTAAG-3'
L'2	5'-(BBQ-650)-GTCAATCGCTTACGGTGAATGGGATCCTCATG--CGAATAGA-3'
C'-DNA	5'-GTCAATCG-3'

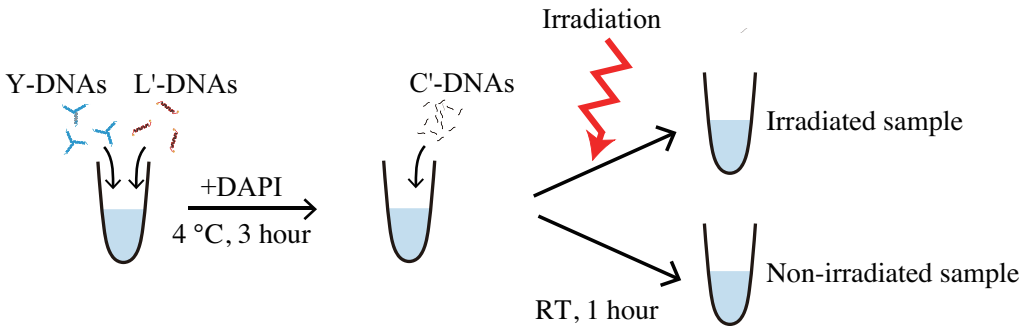

Fig. 3.2 Procedures to prepare the irradiated and non-irradiated DNA solution.

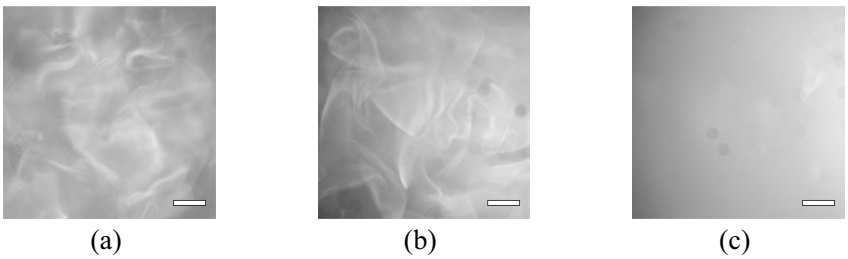

Fig. 3.3 Fluorescence images of a the designed DNA gel (a) in the initial state, (b) without irradiation, and (c) with irradiation for 1hour. Scale bars indicate 200 μm.

3.4 Patterning of DNA gel based on optical decomposition

To demonstrate the patterning of DNA gels in the reverse process of optical formation, the DNA solution was irradiated with several optical patterns generated using a digital mirror device (DMD) and captured using a fluorescence microscope (BX51WI, Olympus Corp.). Figure 3.4 shows the optical set-up used to create patterned DNA gels. A beam emitted from a laser diode (wavelength: 660 nm) was guided to the DMD (Discovery 1100, Texas Instruments, pixel pitch: 13.68 μm) following reflection by two mirrors. The intensity distribution of the laser beam was modulated according to the pattern displayed on the DMD. Passing through the relay lenses, the light intensity distribution, which corresponds to the pattern on the DMD, was imaged at the sample plane. For observation of the fluorescence of DNA gels, the irradiation light was filtered by using two band-pass filters (transmission wavelength: 414–452 nm) and a short-pass filter (transmission wavelength: 500– nm). In this experiment, a sample holder was made of a cover slip, a glass slide, and double-sided tape (Fig. 3.5). The sample was placed in the region surrounded by the double-sided tape and sandwiched between the cover slip and the glass slide. Figure 3.6 (a-d) shows the generated light patterns at the sample plane. The average intensities of the individual light patterns were (a) 570.0, (b) 558.9, (c) 553.0, and (d) 469.2 W/cm^2 on the sample plane. The images of the light patterns and the corresponding fluorescence images were captured using an objective lens with a magnification of 20× (LWD MSPlan20, Olympus Corp.).

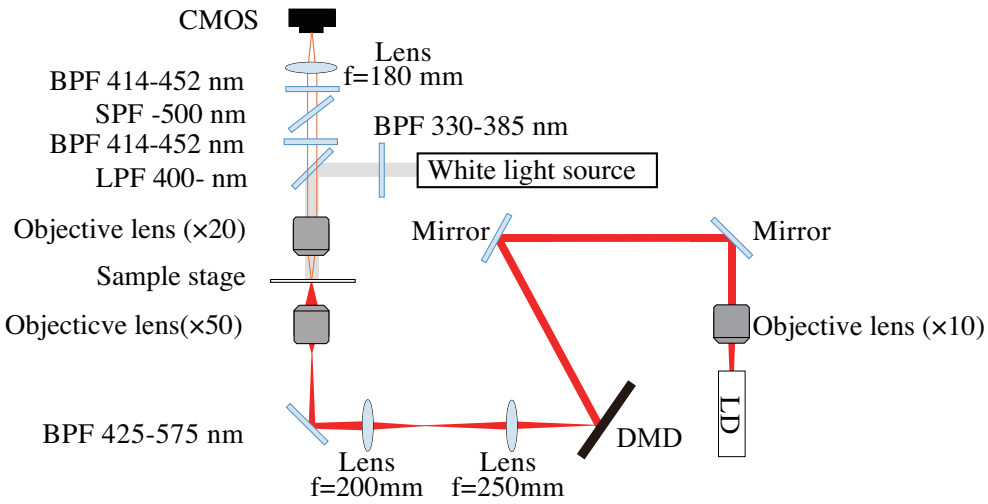

Fig. 3.4 Optical set-up to irradiate a light pattern to DNA gels. LD: laser diode, LPF: long-pass filter, SPF: short-pass filter, BPF: band-pass filter.

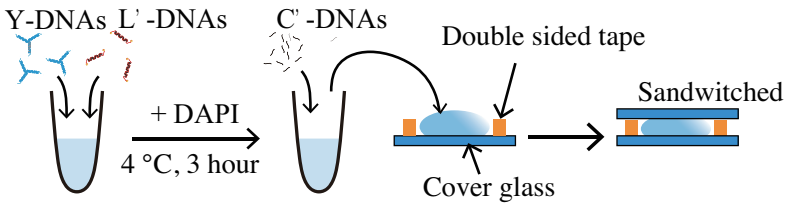

Fig. 3.5 The sample preparation procedure for the patterning of DNA gel by light pattern irradiation.

Figure 3.6 (e-t) shows fluorescence images under light pattern irradiation at each irradiation time (0.0, 50.0, 100.0, and 150.0 s). The fluorescence intensities in the irradiated area are similar to those outside of DNA gels. The intensity profiles on blue and red lines are shown in Fig. 3.6 (u-x). Each intensity profile was normalized with the minimum and maximum intensity values. Moreover, the fluorescence intensity profiles shown in Fig. 3.6 (u-x) were smoothed using a five-point average filter. When the irradiation intensity of light was higher, the fluorescence intensities decreased. From the results, the shape of DNA gels was controlled according to the spatial light intensity distribution.

Interestingly, the fluorescence increased in the irradiation area at the beginning of the irradiation and then decreased [which can particularly be seen in Fig. 3.6 (i)]. This fluorescence persisted even when the irradiation was stopped. A possible reason for this is that quenchers on the L-DNAs went away from the DNA gels, and most of the excitation energy of the DAPI was converted to fluorescence. The quenchers on the L-DNAs can absorb the energy of the DAPI when they are close to it [81]. In the initial state, the DAPI in the DNA gels not only emits fluorescence but also transfers the excitation energy to the quenchers at the same time. When the DNA gels began to be decomposed, the L-DNAs were cleaved from them, and fluorescence of the DAPI in the DNA gels increased due to the absence of quenchers. To investigate whether the intensity of DAPI increases when Y-DNAs are separated from L-DNAs and bind with C'-DNAs, the fluorescence intensity of two DNA solutions at different states was measured using a fluorescence spectrophotometer (JASSO Corp., FP-6200). Two kinds of sample with different procedures were prepared, as shown in Fig. 3.7 (a, b). The first sample contained Y-DNAs and L-DNAs, and the other contained Y-DNAs and C'-DNAs. After mixing DAPI dyes with each of the samples and keeping the temperature at 6 °C for 3 h, C'-DNAs and L-DNAs were added to the individual samples. While Y-DNAs bound with L-DNAs in the DNA solution shown in Fig. 3.7 (a), they bound with C'-DNAs in the DNA solution shown in Fig. 3.7 (b) because C'-DNAs prevent Y-DNAs from binding with L-DNAs. Figure 3.7 (c) shows the fluorescence intensity of the DNA solutions measured immediately after the sample preparation. The irradiation wavelength for excitation of DAPI was 360 nm and the detected fluorescence wavelength was 460 nm. Six samples were prepared for

each procedure and the intensity values were normalized by the mean value for the DNA solution prepared as shown in Fig. 3.7 (a). The fluorescence intensity of the DNA solution containing Y-DNAs binding with L-DNAs was lower than that containing Y-DNAs binding with C'-DNAs. These results show that fluorescence intensity increases when Y-DNAs in DNA gels are cleaved from L-DNAs and bind with C'-DNAs. After sufficient irradiation time, the DNA gels were decomposed because the sticky ends of the Y-DNAs bound to C'-DNA, and the DNAs in the irradiation area were simultaneously dispersed by the thermal gradient generated by the excited quenchers. Therefore, suitable irradiation is required for the decomposition and resulting decrease in viscosity.

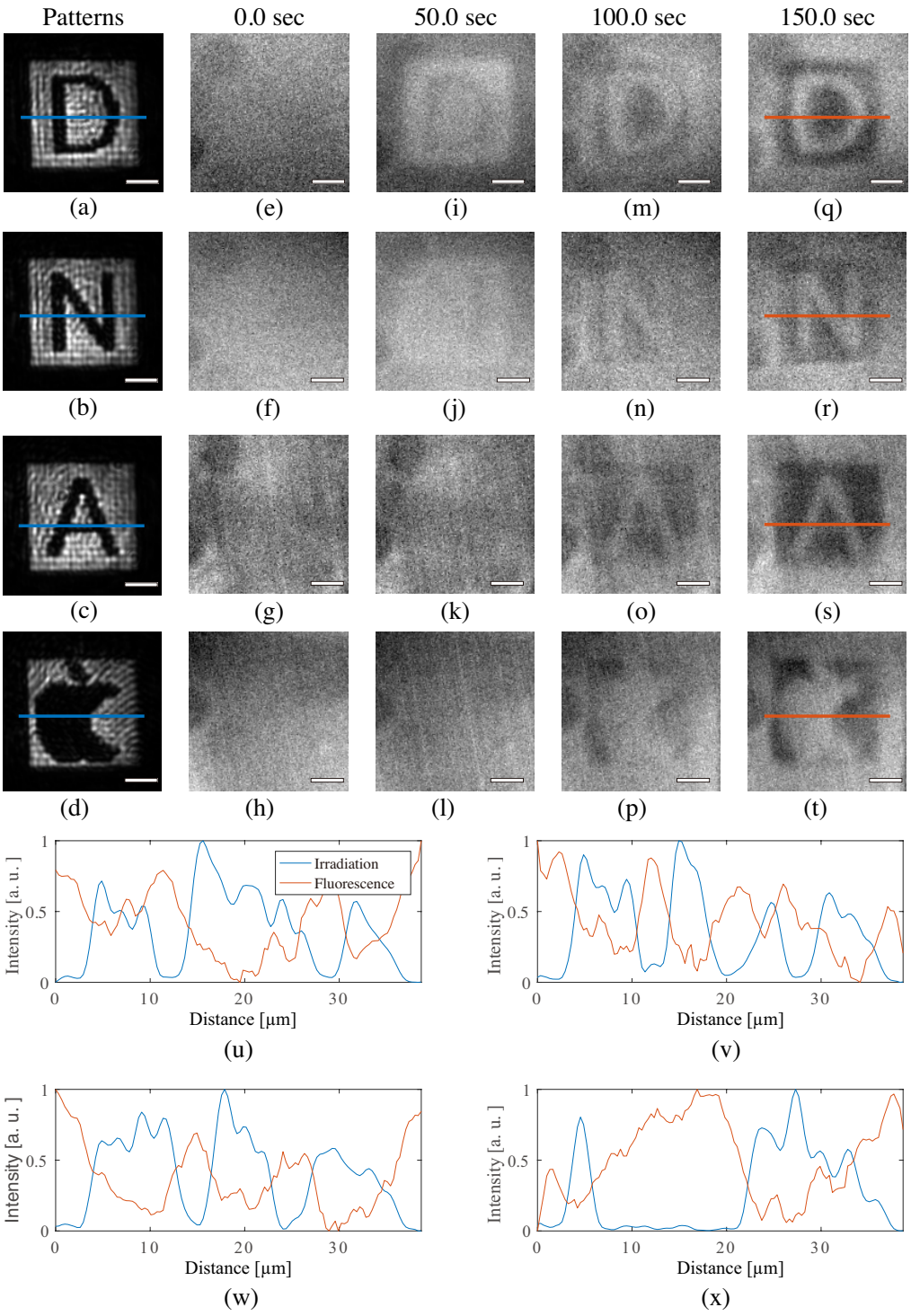

Fig. 3.6 Generated light patterns with the shapes of (a) D, (b) N, (c) A, and (d) a bitten apple. (e-t) Fluorescence images after irradiation for each duration (0.0, 50.0, 100.0, and 150.0 s). (u-x) Intensity profiles of the blue and red lines shown in (a-d) and (q-t), respectively. Scale bars indicate 10 μm.

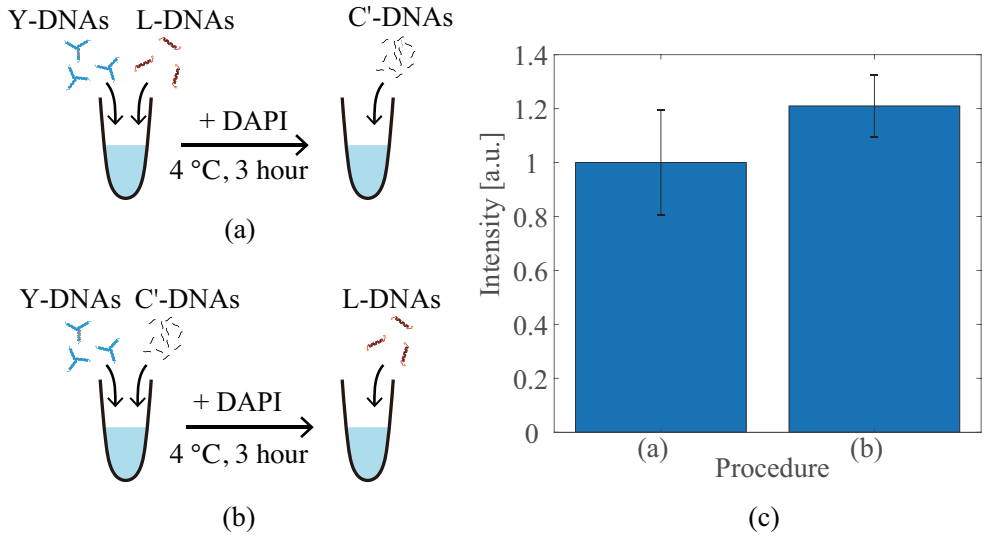

Fig. 3.7 Procedures to prepare DNA solutions in which the Y-DNAs bind to (a) the L'-DNAs and (b) the C'-DNAs. (c) Fluorescence intensity of the samples prepared by the methods shown in (a) and (b). Individual intensities are normalized by the value of method (a).

3.5 Mobility modulation by optical decomposition of DNA gel

The decrease in viscosity caused by spatially controlled optical decomposition of DNA gels can be applied to modify the mobility of micrometer-sized objects. To confirm this, the Brownian motion of polystyrene beads (PSBs) encapsulated in the DNA gels was measured. The preparation procedure to form DNA gels encapsulating PSBs is shown in Fig. 3.8. The DNA gels containing PSBs (07310, Polysciences, Inc., 1.0 μm) were created by mixing the Y-DNA solution with the PSBs and the L-DNA solution. After 3 h and while maintaining the temperature of the DNA solution at 6 °C, the samples were placed on the sample holder and observed at room temperature. Instead of the double-sided tape in the sample holder used in the patterning experiment, additional PSBs of a different size were used (17136-5, Polysciences, Inc., diameter: 10.0μm) to create the gap between the glass slide and the cover slip. This gap limited the movement of the PSBs within the observable depth, and thus the position could be measured. For the decomposition, a square pattern (intensity: 617.3 W/cm^2) shown in Fig. 3.9 (a) was used to irradiate the DNA gels containing PSBs of 1.0 μm in diameter, and bright-field images of the PSBs were captured every 0.35 s. The decomposition of the DNA gels was confirmed from the fluorescence images taken before and after irradiation [Fig. 3.9 (b, c)].

Bright-field images of the PSBs in DNA gels with and without irradiation at each timepoint (0.0, 70.0, 140.0, and 210.0 s) are shown in Fig. 3.9 (d-g) and (h-k), respectively.

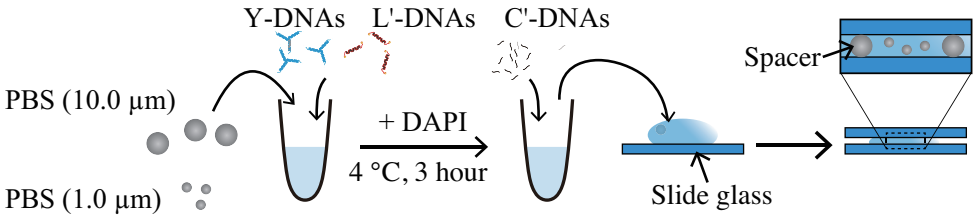

Fig. 3.8 Sample preparation procedure to observe mobility modulation of PSB.

The individual images were captured using the optical set-up shown in Fig. 3.4 (a). The PSBs under irradiation gradually moved, whereas the positions of those without irradiation hardly changed. The displacement distances of five PSBs between each frame were also measured, and the mean and variance of the sum of squared displacements (SSD, r_t) at time t were calculated. The SSD is defined as follows:

$$r_t = \sum_{i=1}^{t} (x(t_i) - x(t_{i-1}))^2, \tag{3.1}$$

where t_i is the time for the i-th frame in a sequence of images, and $x(t_i)$ is the position at t_i. To detect the position of a PSB from individual images, the center of the PSB was obtained by Hough transformation of the images. Figure 3.9 (l) shows the relationship between the mean SSD of the PSBs and the observation time. Each SSD was normalized by using the maximum value of SSDs measured for the sample of the same composition under the conditions without irradiation. Without irradiation, the SSDs increased linearly owing to Brownian motion. In contrast, the displacement with irradiation was higher than that in the case without irradiation, and the rate of increase of the SSD with irradiation became greater as time passed. The normalized SSDs of the PSBs in the DNA gels without the quenchers and in the DNA solution including L-DNAs did not nonlinearly increase even with irradiation. These results show that the degree of Brownian motion increased due to the reduction in DNA gel viscosity caused by thermal energy not from the irradiated light itself but from the excited quenchers. To confirm that the viscosity was modulated according to the irradiation conditions, the SSDs under light irradiation of various intensities were measured. Figure 3.9 (m) shows the mean SSDs under the irradiation conditions with light intensity of 1384.1, 851.7, and 617.3 W/cm^2. The degree of motion of the PSBs increased with increasing light intensity. Furthermore, the diffusion coefficient was obtained using the Stokes-Einstein equation. The dependence of the diffusion coefficient obtained from these measurements on the time is shown in Fig. 3.9 (n). In the calculation, the temperature of the DNA solution was assumed to be room temperature, 23 °C. The diffusion coefficients in DNA gels under conditions with

and without irradiation were measured from the mean square displacement of beads over 10.5 s. The diffusion coefficient rapidly increased after 31.5, 63.0, and 136.5 s, respectively. These results revealed that the DNA gels began to decompose after those times. Dynamic viscosity is inversely proportional to the diffusion coefficient [82]. The viscosity values before and after irradiation with 617.3 W/cm^2 were estimated to be 3.0 and 1.0 mPa·s, respectively. Therefore, the decrease in viscosity can be controlled by adjusting the irradiation conditions, and the mobility of PSBs, which depends on the viscosity, can be temporally modulated by light irradiation. It is thus expected that objects could be guided to given positions by controlling the light pattern design.

3.6 Discussion

In the patterning of DNA gels, the overall size of these gels was 30 μm, which is smaller than that by the optical formation shown in Section 2.5. It is considered that this difference is due to the thermal and molecular dispersion induced by the excited quenchers. In the method, the DNA gel is decomposed by thermal energy generated from the quenchers, and the dispersion effect inevitably occurs. The dispersion effect increases as the light intensity increases. The light intensity in the patterning of DNA gels based on the optical decomposition was approximately 500 W/cm^2, which is one-tenth of that based on the optical formation. Thus, the thermal dispersion effect is reduced and the elaborate control of DNA gels' shape is achieved.

3.7 Conclusion

This chapter presents a physical effect on a micrometer-sized object achieved by a change in the state of a DNA network induced by an optical signal. To demonstrate the capacity of this method, the change in viscosity of DNA gels based on optical decomposition and the modification of the mobility of a micrometer-sized object are presented. The experimental results demonstrated the patterning of DNA gels on a micrometer scale using light pattern irradiation. Moreover, the light irradiation was effective to decrease the viscosity of DNA gels and enhance the degree of motion of PSBs. The results indicate that the mobility of micrometer-sized objects can be modulated at the desired position and time via the optical control of a DNA network. This method provides a new approach for controlling the motion of micrometer-sized objects.

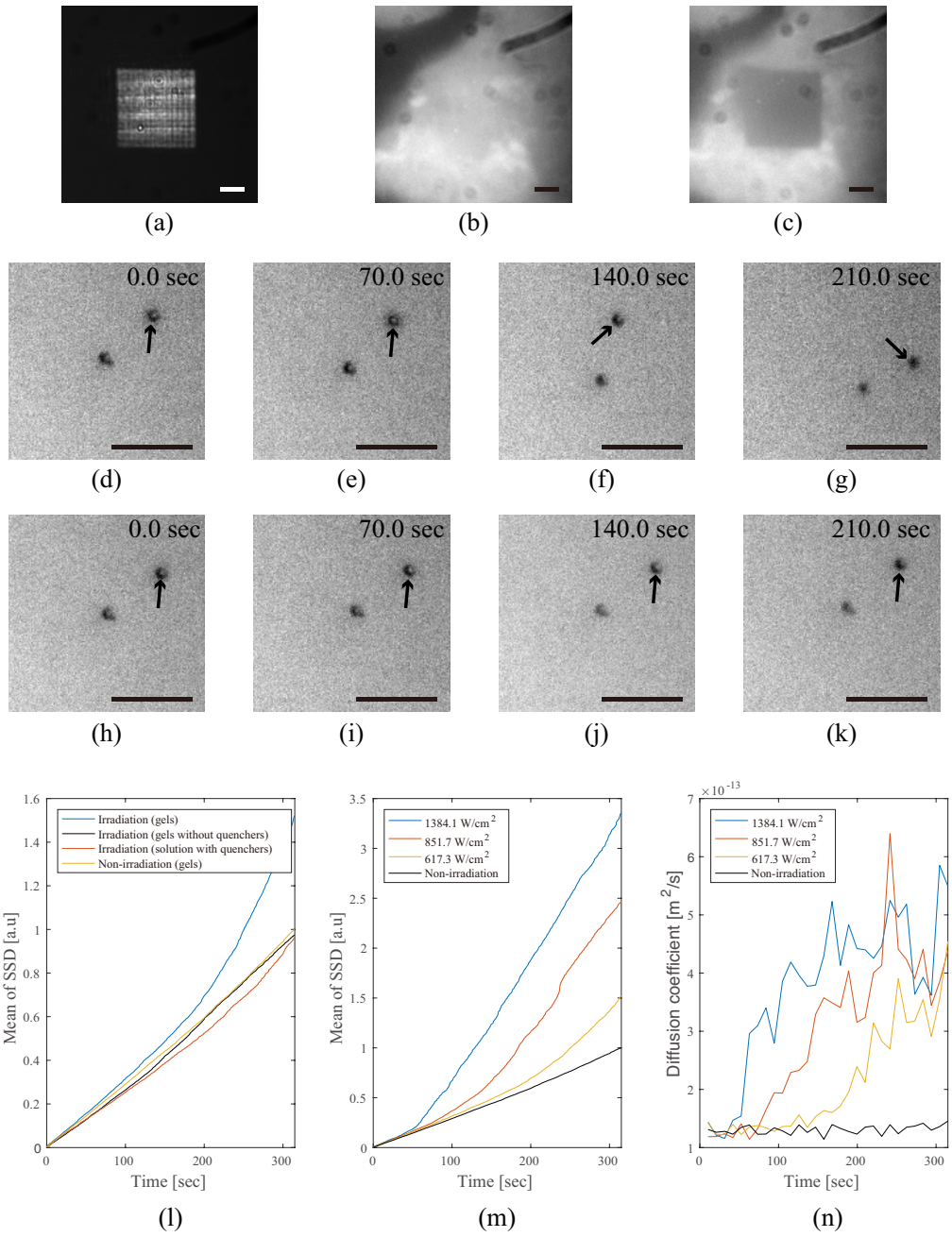

Fig. 3.9 (a) Light pattern to decompose DNA gels. Fluorescence images obtained (b) before irradiation of the irradiation pattern and (c) after the irradiation for 310.0 s. Bright-field images (d-g) under the irradiated and (h-k) and unirradiated conditions for each time (0.0, 70.0, 140.0, and 210.0 s). The same PSB is indicated by black arrows. Scale bars indicates 10 μm. The mean of SSD depending on (l) the sample conditions and (m) the irradiation intensity. (n) The relationship between the observation time and the spatial diffusion coefficient of the DNA solution.

Chapter 4

Spectro-temporal signal generation using quantum dot network

4.1 Introduction

QDs transform an optical signal into a fluorescent signal. Furthermore, the fluorescent signal can be modulated using FRETs located between QDs [62]. The use of a combination of QDs is effective to increase the types of fluorescent signal compared with when a single QD is used, and diverse spectral and temporal signals can be generated [83]. The diversity of the signals in the wavelength and time domains contributes to classifying the object information and optical input. The attachment of combined QDs to molecules is useful for observing multiple types of cell [84, 85]. The fluorescent signals of QDs modulated by optical inputs can be applied for nanoscale computing [86–89]. However, the previous methods require a complicated procedure to accurately control QDs' arrangements. To create the variation of fluorescent signals, it is effective to construct a system generating multistep FRET between QDs at multiple locations and times simultaneously. By generating multistep energy transfer through FRETs between QDs, the energy state of QDs is modulated dynamically according to the optical input, and various temporal and spectral signals can be generated. This system in which QDs communicate with each other via energy provided by optical input can be regarded as a networking system consisting of QDs.

In this chapter, a method to generate diversity of fluorescent signals using a QD network connected by FRET pathways is presented. The QD network is constructed by inducing FRETs in randomly distributed QDs. The method enables us to construct large-scale QD networks because no nanofabrication techniques are required. Moreover, as a result of multistep FRETs between the QDs, the energy state of each QD is changed; this leads to the dynamics of spectral signals. In Section 4.2, the signal generation mechanism by construction of a QD network is described. In Section 4.3, the diversity of spectral signals from randomly distributed QDs depending on the irradiation area is confirmed.

Section 4.4 shows the temporal signals from randomly distributed QDs depending on the irradiation intensity and its wavelength.

4.2 Signal generation using QD network based on multistep FRET

Figure 4.1 shows a schematic diagram of the signal generation using a QD network. The QD network consists of several types of QD, which generate fluorescence with different wavelengths. When irradiated with the excitation light, QDs generate fluorescence. The QDs are excited according to the irradiation conditions and generate fluorescence stochastically. In the QD network, QDs are spatially distributed and the distances between adjacent ones have nanometer order of variation. The size of the distribution can be extended to the millimeter order. When the randomly distributed QDs are irradiated with excitation light, some of them generate fluorescence. At the same time, other excited QDs transfer the excitation energy to nearby QDs by FRET. The QDs have a dense distribution, so multiple steps of FRET can be induced. Because the multistep FRETs change the energy state of the QDs in the network, the fluorescent signal from each QD is modulated dynamically. The QDs excited by light irradiation differ according to the irradiation conditions, and various spectral signals are generated depending on the FRET pathways induced optically. Furthermore, when the QDs accepting the excitation energy are excited, the level occupancy effect should be considered. Owing to this phenomenon, the FRET pathways are changed and the fluorescent signals are further modulated. The level occupancy effect can be induced depending on the irradiation conditions. Therefore, the temporal and spectral signals from the QD network are modulated depending on the optical signals.

4.3 Spatio-spectral signal variation depending on the irradiation position of aggregated QDs

The QD network provides a diversity of spectral signals depending on the irradiation area. To investigate the construction of the QD network, the spectral signals of the QD aggregation at individual irradiation areas were measured. Figure 4.2 shows the procedure for preparing the randomly distributed QDs. In this experiment, QD490, QD525, and QD575 (753904, Sigma-Aldrich, fluorescence wavelength: 490, 525, and 575 nm, respectively) were used as network components. Each QD was composed of CdSeS/ZnS. The QD solution including individual QDs was prepared and dropped on a slide glass. By drying this solution, a QD aggregation in which the QDs were randomly distributed on the nanoscale was formed.

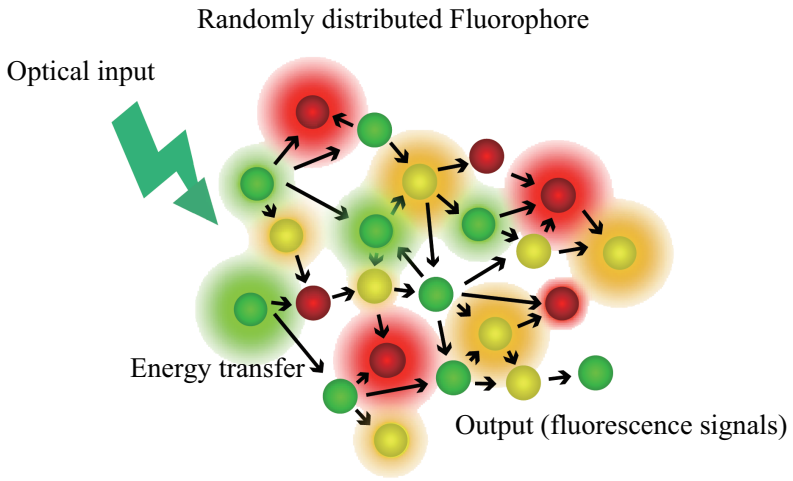

Fig. 4.1 Schematic diagram of signal generation from QD network

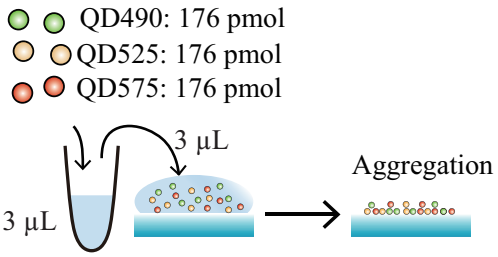

Fig. 4.2 Sample preparation method to make the QD aggregation

The optical set-up to measure the spectral signals is shown in Fig. 4.3. A laser beam emitted from a light source (OBIS FP 405LX, Coherent) passes through a relay lens and is focused on the sample plane using an objective lens (UPLFN40X, Olympus). The fluorescence generated by the optical excitation of QDs enters a multimode optical fiber through a relay lens. The light passing through the multimode fiber is detected by a spectrometer (Glacier X, BWTEK) and the spectral signal is measured. The sample was irradiated by light with intensity of 1.43×10^{-4}W/cm^2, and the diameter of the focused laser beam with a circular intensity distribution was 658.8 nm. The fluorescence spectrum was obtained while displacing the sample by 50 μm.

Figure 4.4 (a) shows the spectra of the randomly distributed QDs at different irradiation positions. Various spectra were obtained at each position. To investigate the change of fluorescence emitted from each type of QD, the intensity data at the fluorescence wavelength of three types of QD were selected [Fig. 4.4 (b)]. The intensity was normalized so that the minimum and maximum intensities were 0 and 1. At the individual irradiation

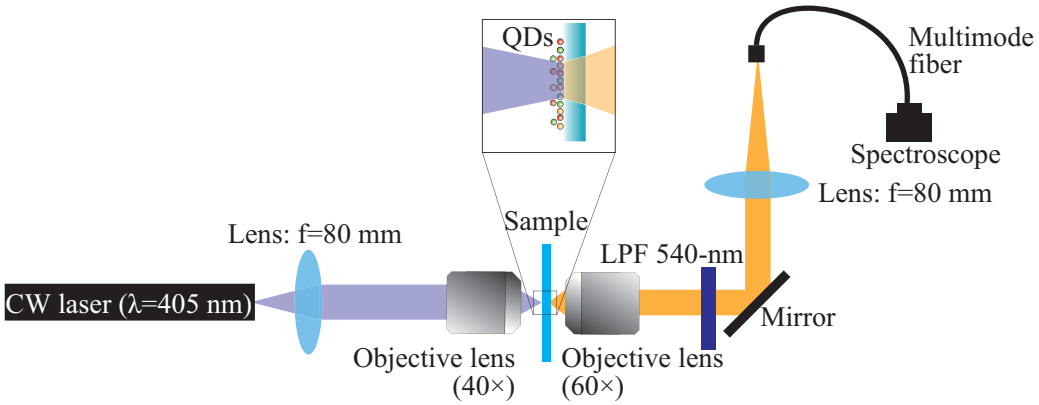

Fig. 4.3 Optical set-up for measuring the spectral signal from the QDs.

positions, the different intensities were measured for all fluorescence wavelengths. The reason for the different signal generation at each irradiation area is shown in Fig. 4.5. When the QDs are distributed randomly, the network structure in each irradiation area varies. Corresponding to the structure, the different FRET pathways are generated and specific spectral signals are generated. The results indicate that the difference of transfer pathways in the QD network contributes to modulating the fluorescence signals, and various spectral signals are generated from the randomly distributed QDs depending on the irradiation area.

4.4 Temporal signal variation of QD ensemble depending on the irradiation conditions

To confirm that the FRET pathways in the QD network are modulated depending on the irradiation conditions, the temporal signal of a QD ensemble depending on the irradiation intensity and its wavelength was measured. Using the sample preparation method shown in Fig. 4.2, the QDs were aggregated. The QD aggregation has a much higher density of QDs and hence the signal variation according to the network structure is small, although diverse spectra are obtained by the experiment shown in Section 4.3. To increase the variation of the temporal signals from the QD network, the QD ensemble using resin was prepared [Fig. 4.6 (a)]. QD540 and Q580 (CZ540-10 and CZ580-10, NN-LABS, LLC, fluorescence wavelengths: 540 and 580 nm, respectively) were included in the resin solution. The sample was dropped on a slide glass and was spread using a spin coater. By spreading the solution, the QDs were scattered. After rotation at 500 rpm for 100 s, the sample was heated at 120 °C for 10 min to cure the resin. The efficiency of FRET working between QD540 and QD580 was higher than that between QD580s. To investigate the

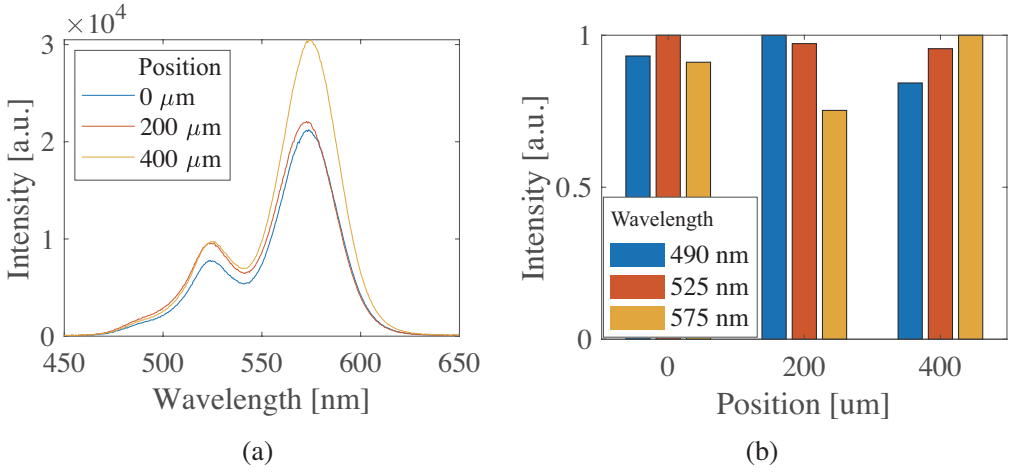

Fig. 4.4 (a) Fluorescence spectra of randomly distributed QDs at relative positions of 0, 200, and 400 μm. (b) Relationship between the irradiation position and the fluorescence intensity of wavelengths of 490, 525, and 575 nm.

effect of FRET, a sample made only of QD580 was also prepared by the same procedure [Fig. 4.6 (b)].

The optical set-up to measure the temporal signal from the QD ensemble is shown in Fig. 4.7. Pulsed light that is emitted from a light source (Mai Tai, Spectra-Physics, pulse width: 80< fs, repetition frequency: 1.0 kHz) passes through an optical parametric oscillator (TOPAS Prime, Spectra-Physics) and a wavelength converter (NirUVis, Spectra-Physics), and the irradiation wavelength is modulated. After reflecting with two mirrors, the light is linearly polarized by a polarizer. The polarized light is focused on the sample plane using the objective lens (PLN10X, Olympus). Fluorescence photons generated by optical excitation of the QDs enter the objective lens and are reflected by

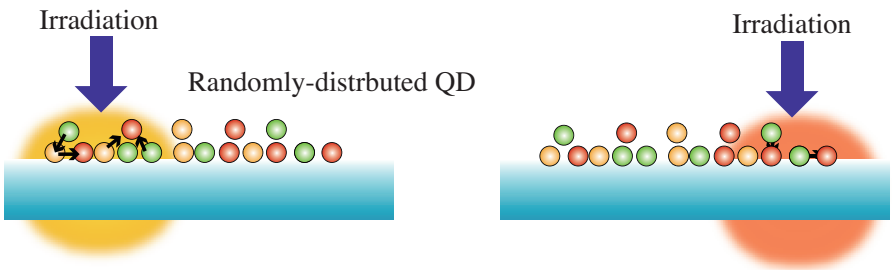

Fig. 4.5 Diverse spectral signals generated by the different FRET pathways.

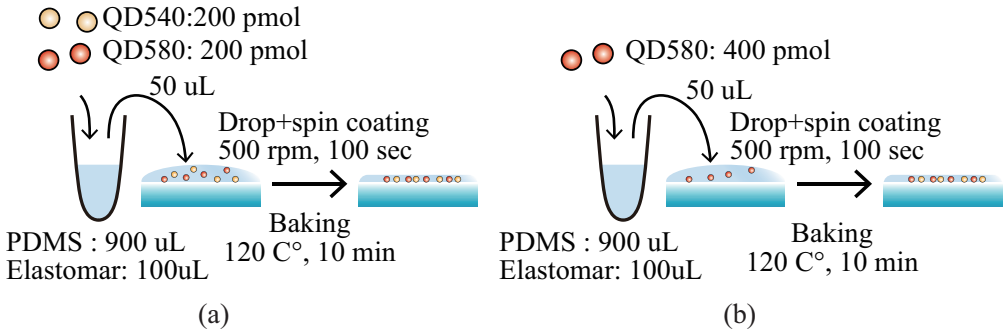

Fig. 4.6 Procedure to prepare a QD ensemble consisting of (a) QD540+QD580 and (b) QD580 alone.

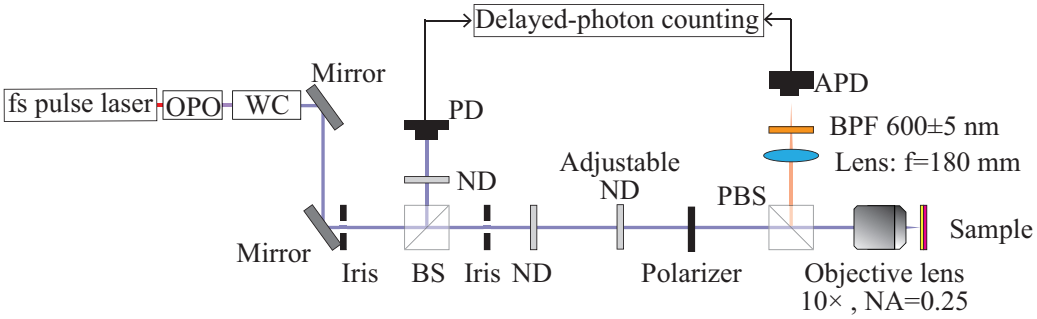

Fig. 4.7 Optical set-up to measure temporal signals depending on the irradiation conditions. OPO: optical parametric oscillator. WC: wave convertor.

a polarization beam splitter; then, the photons are detected using an avalanche photodiode (Nippon Roper, NR-K-SPD-050-CTE). The temporal signals from the sample are obtained by measurement of the time difference between the trigger signal entering a photodiode (ET-2030, EOT) and the fluorescence photon. In the experiment, the irradiation area was $2.0 \times 2.0 \mu m^2$, and the irradiation wavelength was 400 nm. A band-pass filter (transmission wavelength: 600±5 nm) was employed to obtain the fluorescence signal from QD580.

4.4.1 Temporal decay depending on the irradiation intensity

Figure 4.8 (a) shows the fluorescence decay at different irradiation intensities. The time resolution of the fluorescence decay was 12.0 ps. The temporal signals were measured at different irradiation positions three times. The fluorescence decay is faster as the light intensity decreases. To reveal the relationship between the signal decay and the irradiation intensity, the decay rate was evaluated. Multistep FRET frequently occurs within a few picoseconds from the time of irradiation, so individual temporal signals from 0.0 to 0.20

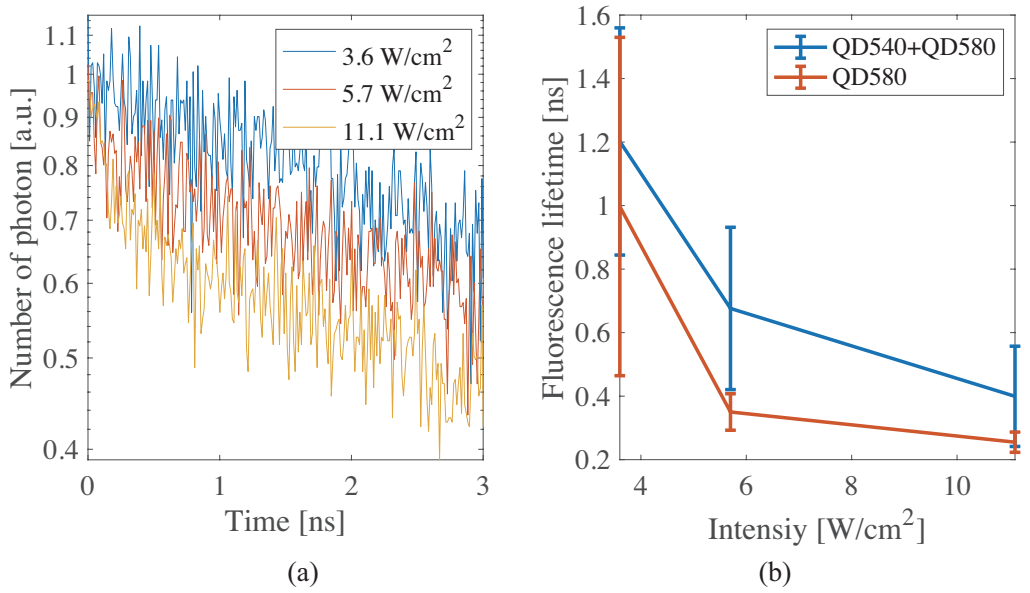

Fig. 4.8 (a) Fluorescence decay under irradiation with different intensities. Each decay is normalized so that the maximum photon number is 1. (b) Fluorescence lifetime τ of the QD ensembles at each irradiation intensity.

ns were selected and fitted with a function of time $f(t) = A\exp(-t/\tau) + b$ by using the nonlinear least squares method. The constant τ represents the fluorescence lifetime, which is the time when the number of photons is $1/e$ of the maximum. Figure 4.8 (b) shows the dependence of the average fluorescence lifetime on the irradiation intensity. The fluorescence lifetime for both samples rapidly decreased as the intensity increased. The results show that the temporal signals were modulated depending on the irradiation intensity.

A possible reason for this is that the modulation is induced by the different FRET pathways due to the level occupancy effect between QDs. Figure 4.9 shows the process of fluorescence decay depending on the irradiation intensity. Among the randomly distributed QDs, some of them adopt an excited state due to the irradiation, and the number of excited QDs depends on the irradiation intensity. The excited QDs retain the energy for a few nanoseconds and then generate fluorescence. The duration of energy retention is stochastic, and the fluorescence intensity decreases exponentially with time. Multistep FRETs are also induced from the excited QDs to unexcited ones [Fig. 4.9 (a)]. In the case of high irradiation intensity as shown in Fig. 4.9 (b), the number of excited QDs increases. The excited QDs attempt to transfer energy through FRET. At the same time, the level occupancy effect can induce Auger recombination [67]. This phenomenon transfers the excited electrons in the acceptor QD to higher energy levels. These transferred electrons at higher energy levels return to their previous energy levels via the nonradiative

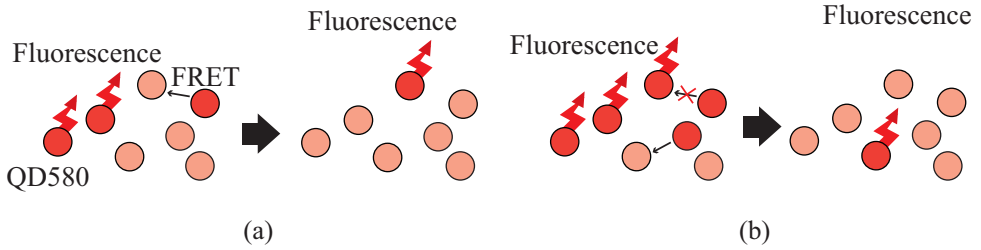

Fig. 4.9 Process of fluorescence decay of randomly distributed QDs in cases of (a) low and (b) high irradiation intensity.

relaxation process [90]. As a result, the energy transferred through FRETs is released as thermal energy. Thus, the energy preserved in the QD network is rapidly consumed, and the fluorescence decay becomes faster as the irradiation intensity increases. Auger recombination is more frequently generated by increasing the number of QDs in the excited state [31], and the experimental result supports this phenomenon. Therefore, the results indicate that temporal signals are modulated due to the change of FRET pathways.

4.4.2 Temporal decay depending on irradiation wavelength

Next, the temporal signals generated using different irradiation wavelengths were measured. The temporal signals were measured at different irradiation positions with individual irradiation wavelengths three times. The intensity of the pulse was 5.7 W/cm^2. Figure 4.10 (a) shows the relationship between the irradiation wavelength of the input pulse and the temporal signal from the sample. As the irradiation wavelength increased, the fluorescence decay became faster. To evaluate the degree of modulation of the fluorescence decay, the temporal signals from 0.0 to 0.20 ns were picked up and fitted with a function of time, $f(t) = A\exp(-t/\tau) + b$, by using the nonlinear least squares method. Figure 4.10 (b) shows the average fluorescence lifetime on the irradiation wavelength. The lifetime of the QD ensemble with only QD580 changed little for the irradiation with different wavelengths. In contrast, the lifetime of the QD ensemble including QD540 and QD580 decreased by using longer irradiation wavelengths. This shows that high FRET efficiency by using multiple types of QD is associated with a change in lifetime. Moreover, the lifetime of the QD ensemble including QD540 and QD580 under irradiation exhibited variation. The diversity of the temporal signal depending on the irradiation area was also demonstrated.

A possible reason for the difference in the manner of modulation of temporal signals is the difference of FRET pathways due to the QD excitation depending on the irradiation wavelength. Figure 4.11 (a) shows the excitation spectrum of the resin with QD540 and

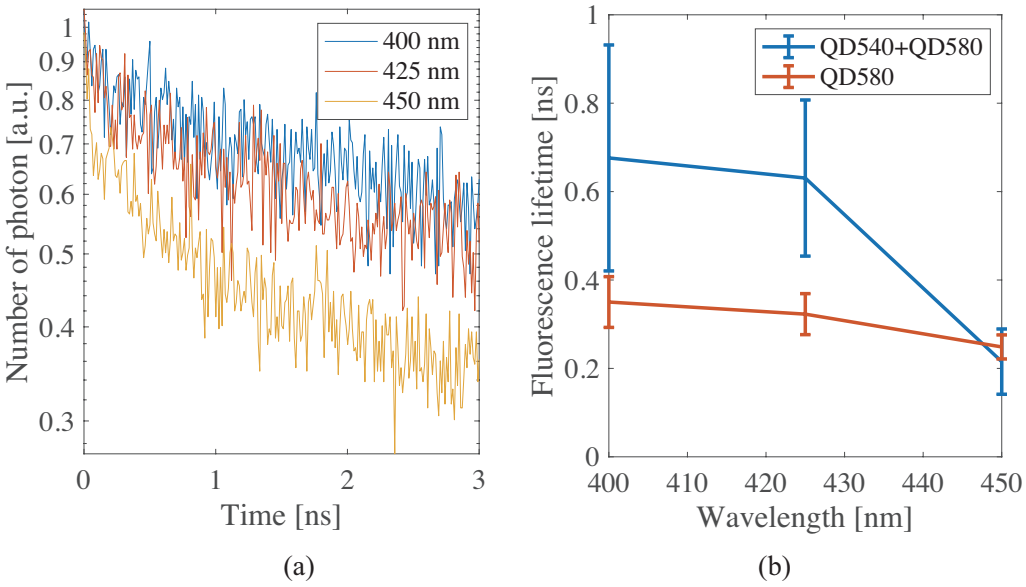

Fig. 4.10 (a) Fluorescence decay under irradiation with different wavelengths. (b) Average fluorescence lifetime τ of the QD ensembles at each irradiation wavelength.

that with QD580. The spectrum was obtained using a fluorescence spectrophotometer (LS45, PerkinElmer). The detection wavelengths of QD540 and QD580 were 564.5 and 607.5 nm, respectively. Each value was normalized to the fluorescence intensity value under irradiation with a wavelength of 400 nm. The excitation spectrum is related to the absorption spectrum, and the fluorescence intensity depends on the number of QDs excited by the irradiated light. When the irradiation wavelength is 400 nm, both QDs absorb a substantial amount of energy; then, the energy of QD540 is transferred to QD580 through FRETs [Fig. 4.11 (b)]. As a result, the excited energy state of QD580 is maintained for a long time, and the fluorescence decay becomes longer. As the irradiation wavelength becomes longer, the number of excited QD540s decreases rapidly compared with that of QD580. This means that the number of QD540s decreases and the amount of transfer energy by FRET decreases [Fig. 4.11 (c)]. As a result, the fluorescence decay of QD580 becomes short. These results indicate that the generation of multistep FRETs is controlled in a manner dependent on the irradiation wavelength, and diverse temporal signals can be generated.

4.5 Conclusion

The signal generation method using randomly distributed QDs is presented. The spectral and temporal signals from the randomly distributed QDs can be modulated through multistep FRET pathways and the level occupancy effect. The experimental results show

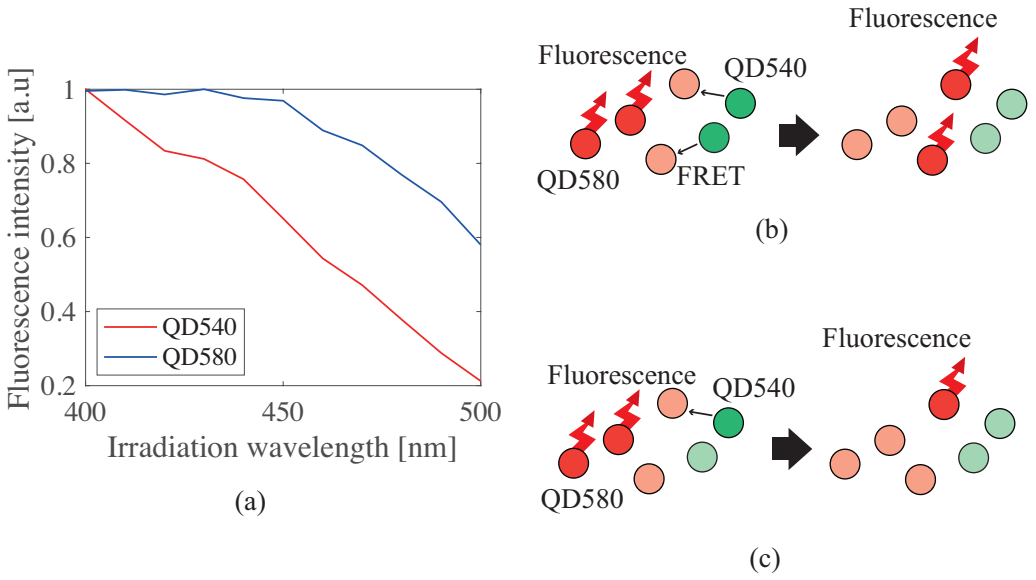

Fig. 4.11 (a) Excitation spectrum of QD540 and QD580. Process of fluorescence emission of the randomly distributed QDs with QD540 and QD580 when the irradiation wavelength is (b) 400 nm and (c) 450 nm.

that the QD aggregation creates various spectral signals at different irradiation areas. Moreover, the FRET pathways can change due to the energy occupancy effect and the difference in the number of excited QDs. Temporal signals can consequently be modulated depending on the irradiation intensity and wavelength. The results indicate that the use of a QD network is effective for generating various signals by optical control.

Chapter 5

Possibility of temporal information processing using quantum dot network

5.1 Introduction

Quantum dot (QD) networks provide diverse signals depending on the irradiation conditions. Depending on the sequential optical inputs, each QD's energy is modulated dynamically. This modulation generates the dynamics of fluorescence signals. The dynamics makes it possible to map the temporal signals to a hyperplane. Hence, the use of dynamics realizes the classification of input data [91]. The diversity of temporal signals from the QD network provides different types of dynamics, which can be used for temporal information processing. The temporal data prediction using physical phenomena provides a low-energy-consumption system with a small size. The size of the QD network ranges from a few nanometers to a few micrometers, which is smaller than an electrical circuit implementing data processing. Furthermore, a use of light provides high-speed processing owing to the speed of light. Therefore, temporal information processing using a QD network has the potential to realize a high-speed system on the nanometer scale.

This chapter presents the possibility of achieving information processing using a QD network. The signal modulation due to the dynamic change of QDs' energy in the QD network has the potential to discriminate temporal information of optical input. By analyzing the output from the QD network, the prediction of temporal signals is achievable. To investigate the validity of the method, a mathematical model of a QD network is constructed. By calculation using the model, the diversity of temporal signals from the QD network is reproduced and is applied to the classification of temporal data. Section 5.2 shows a mathematical model of a QD network representing a diversity of temporal signals. Section 5.3 describes the simulation results of temporal signals generated from QD networks using pulse light with different irradiation conditions. Section 5.4 shows

a temporal information processing system utilizing QD networks. Section 5.5 presents a discussion about the feasibility and scalability of the proposed system.

5.2 Mathematical model of a quantum dot network connected by FRETs

To investigate the performance of the temporal information processing using the diversity of temporal signals from QD networks, a mathematical model of a QD network generating fluorescence was constructed. The model of a FRET-based network is described using a master equation [92]. By considering characteristics of a QD, a model of the QD network is constructed. First, the energy change of the QDs in the network is considered. Figure 5.1 shows a Jablonski diagram indicating the transfer process of electrons in a QD existing in the network. The numbers of the electrons at the ground and excitation levels are denoted as N_e and N_g, respectively. The total number of electrons in the QD is constant ($N_e + N_g = \mathrm{N}$). By optical excitation, some of the electrons in each QD of the network are transferred to excitation levels, and N_e increases. The electrons in the excited state return to the ground level via radiative and nonradiative relaxation processes. At the same time, the number of electrons the in i-th QD, which is an element of the QD network, changes as a result of FRET with the j-th QD, which is nearby i-th QD. When many electrons are at excited levels, Auger recombination [67] is often induced due to the level occupancy effect. The electrons in the acceptor QDs thereby transfer to higher energy levels, while those in the donor QDs return to the ground level. The QD network includes excited and unexcited QDs. Depending on the FRET pathways, the number of excited electrons changes and sometimes becomes saturated. In several studies, it has been assumed that the electrons in a QD transfer to several energy levels [31, 93–95]. For simplification of the mathematical model, a two-level system of the electrons in a QD is considered in the proposed model. The rate equation of excited electrons $N_{e,i}$ in the i-th QD considering the FRET and level occupancy effect is written as follows:

$$\frac{dN_{e,i}}{dt} = \frac{\sigma I_{ex}(t)}{h\nu_i} N_{g,i} - k_{r,i} N_{e,i} - k_{nr,i} N_{e,i} - \sum_{i \neq j} k_{i \to j} N_{e,i} + \frac{N_{g,i}}{N} \sum_{i \neq j} k_{j \to i} N_{e,j}. \tag{5.1}$$

Here, $I_{ex}(t)$, σ_i, h, and ν are the irradiation photon density for the excitation of an electron at time t, an absorption coefficient of the QD, the Planck constant, and the frequency of fluorescence from the QD, respectively. k_r and k_{nr} are rate constants of radiative and nonradiative relaxation processes, respectively. $k_r = Q/\tau$ and $k_{nr} = (1-Q)/\tau$, where Q is the quantum yield and τ is the fluorescence lifetime. The first term of Eq. (5.1) indicates the optical excitation, and the number of electrons transferring to the excitation level depends on the number of the electrons at the ground level N_g. The second and third terms indicate the energy emission by radiative and nonradiative relaxation processes,

and the transfer rate depends on the number of electrons at the excitation level N_e. The fourth term denotes the FRETs between the i-th and the j-th QDs. FRET is explained by Förster theory [62], and rate equation modeling FRET is represented [96]. Using the theory and the equation, the rate constant of FRET is described as follows:

$$k_{i\to j} = \frac{1}{\tau_i}\left(\frac{R_0(i,j)}{R(i,j)}\right)^6, \tag{5.2}$$

where $R_0(i,j)$ is the Förster distance determined by Eq. (1.2), and $R(i,j)$ is the distance between the i-th and j-th QDs. The fifth term of Eq. (5.1) indicates Auger recombination induced by FRET. When few electrons are at the ground level, Auger recombination is frequently induced, and the electrons in the acceptor QD transfer to the higher energy levels and then return by the nonradiative relaxation process [31, 67]. The time until returning from the higher energy levels is on the order of a few picoseconds [68]. In the simulation of the two-level system, the transition to higher energy levels is regarded as a very rapid process, so it is assumed that the excited electrons in the acceptor remain at the excitation level. As a result, the electrons transferring to the excitation level by FRET decrease when the electrons at the ground level decrease. The fluorescence signal from the QD network is the sum of radiative energy generated from each QD. Therefore, temporal fluorescence intensity $f(t)$ from the QD network is described as follows:

$$f(t) = \sum_i \left(k_{r,i} N_{e,i}(t) \times h\nu_i\right). \tag{5.3}$$

Eq. (5.3) indicates that the temporal signal shows the dynamics depending on the energy state of each QD. Using Eqs. (5.1) and (5.3), the temporal signals according to a sequential optical input can be obtained.

5.3 Numerical simulation of temporal signals generated from a QD network

To investigate whether the simulation can explain the experimental results shown in Section 4.4 and to demonstrate the validity of the simulation, the temporal signal from the randomly distributed QDs was estimated for irradiation intensity. In the simulation, the distribution of two types of QD (QD_D and QD_A) was restricted to two dimensions for simplification of the analysis (Fig. 5.2). The size of the QD network and the density of QDs were assumed to be 50×50 nm and 4×10^{-3}number/cm^2, respectively. The ratio of the number of QD_D to QD_A in the network is random; however, the QD network consisting of a single type of QD was not considered. The position of each QD was also randomly determined so that the QDs did not overlap with each other. Parameters to calculate Eq. (5.1) are shown in Table 5.1 and Fig. 5.9 in the Appendix. To obtain

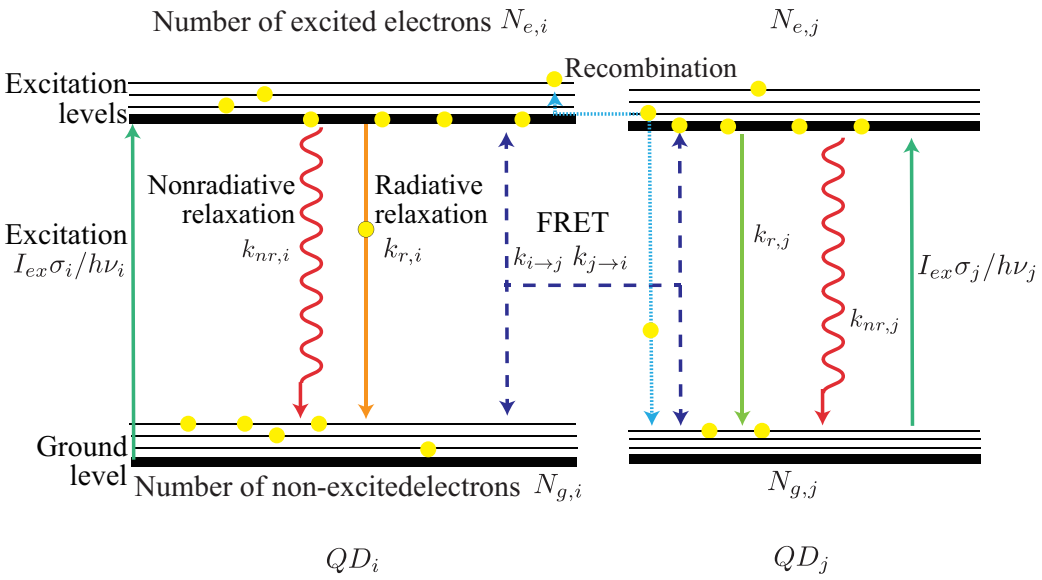

Fig. 5.1 A Jablonski diagram of the QDs in the QD network.

the Förster distance between QD_D and QD_A, the refractive index in the environment was determined as 1.44, which is the index of silicon resin. The orientation factor κ_{ij}^2 between the n-th and j-th QDs was set to 2/3 because of the random anisotropy due to the random distribution of the QDs. The saturation energy is much higher than the energy of an electron, and the energy modulation of QD is considered to be continuous. To output the temporal signal from the network, irradiation of pulse light (width: 74 ps) was assumed. The spatial intensity distribution of the light is uniform because the QD network is smaller than the irradiation area limited by the diffractive limit. The time step to calculate Eq. (5.1) was 10 ps, and the detection wavelength was set to 600 nm, which is the fluorescence wavelength of QD_A. The fluorescence intensity at each time is calculated using N_e obtained from Eq. (5.1) and Eq. (5.3).

Figure 5.3 (a) shows the simulation result of the temporal signal depending on the irradiation intensity. The irradiation wavelength was assumed to be 400 nm. Each value was obtained by setting the peak intensity of the pulse light to $\alpha \times I_{sat,D}$. Here, α is the amplification rate and $I_{sat,D}$ is the intensity value that induces the energy saturation of QD_D. As the intensity increases, the fluorescence decay becomes faster. This relationship is similar to the experimental results shown in Fig. 4.8 (a). To evaluate the decay change, an independent simulation was run 100 times, and the average fluorescence lifetime was measured by fitting a function $f(t) = A\exp(-t/\tau)$ to each temporal signal. Figure 5.3 (b) shows the relationship between the average fluorescence lifetime τ and irradiation intensity. This lifetime decreased nonlinearly by increasing the amplification rate. The decay also decreased nonlinearly in the experiment. This supports the proposed model

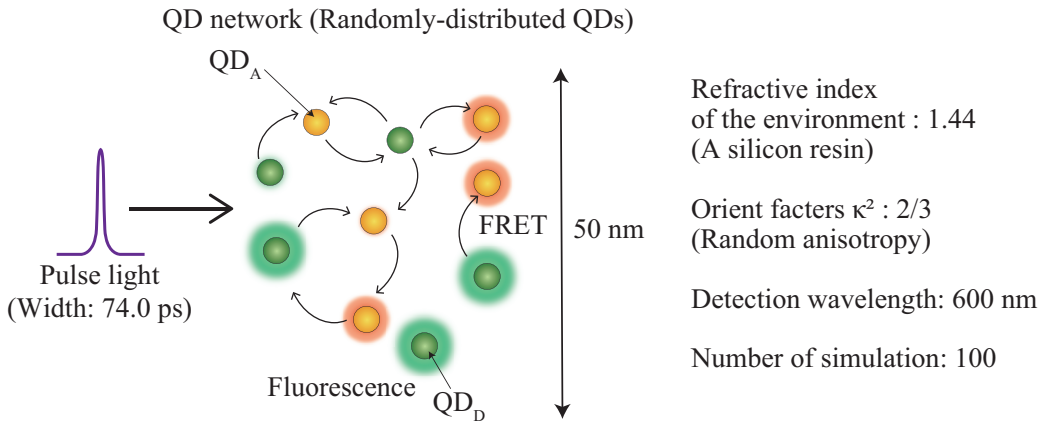

Fig. 5.2 The simulation conditions of a QD network.

qualitatively. Moreover, the standard deviations of the lifetime at each amplification rate (1.0, 10.0, and 100.0) were 0.27, 0.29, and 0.59, respectively. The deviation indicates the variation of the temporal signal according to the network structure. The results show that the signal variation can be increased by the light intensity. The reason for this is that the difference in FRET efficiency according to the network structure becomes noticeable as the irradiation intensity increases. When the QD network is irradiated with excitation light with high intensity, most QD energy is saturated and Auger recombination is frequently induced by FRET. The FRET efficiency is highly dependent on the distance between the QDs (as shown in Eq. 1.1). As a result, the energy state of the QDs in the network is strongly modulated by substantial Auger recombination, and the variation of the temporal signal according to the network structure becomes remarkable.

Next, the relationship between the fluorescence decay and the irradiation wavelength was investigated. Figure 5.4 (a) shows the fluorescence decay at different wavelengths. The amplification rate of the irradiation intensity was 1.0. When the irradiation wavelength is long, the decay becomes faster. Furthermore, the simulation was run 100 times, and the average fluorescence lifetime was measured. The dependence of the average fluorescence lifetime on the irradiation wavelength is shown in Fig. 5.4 (b). The lifetime decreases as the irradiation wavelength becomes longer. In the experimental results shown in Fig. 4.10, the fluorescence lifetime also decreases. This shows that the proposed model can reproduce the experimental conditions qualitatively. The standard deviations of the lifetime at each irradiation wavelength (400, 425, and 450 nm) were 0.25, 0.16, and 0.13, respectively. The QDs absorb more energy for shorter irradiation wavelengths. As the irradiation wavelength increases, it is difficult for the QDs to reach a saturated state, and Auger recombination hardly occurs. As a result, the diversity of the temporal signal depending on the network structure becomes lower upon increasing the irradiation wave-

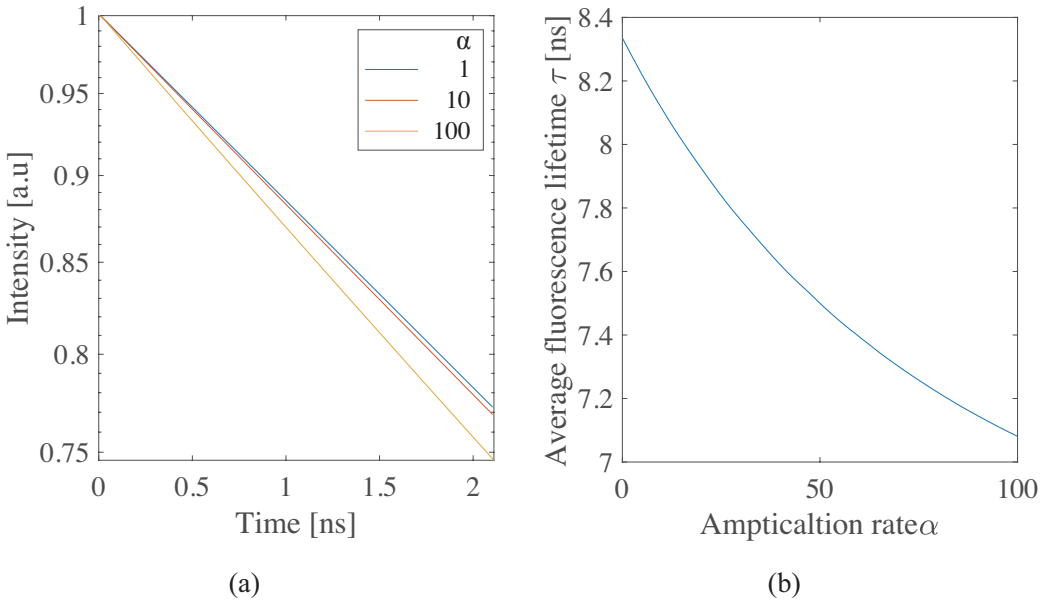

Fig. 5.3 (a) Simulation results of the fluorescence intensity at the irradiation wavelength of the pulse light. The intensity was normalized so that the maximum value is 1. (b) Dependence of the average fluorescence lifetime on the irradiation wavelength α.

length. The results reveal that the variation of temporal signal can be modulated by the irradiation conditions.

5.4 Time-series data prediction using temporal signal from QD network

To demonstrate the capacity for temporal information processing, prediction of a 2-bit XOR task was investigated by simulation. The 2-bit XOR task is used as a benchmark for header recognition in telecommunications [97–99]. In this task, the 2-bit XOR signal x[t], which is a single-bit signal, is determined by the previous ones x[t-1] and x[t-2]. The prediction is not achievable by only linear regression of the data set. To predict the signal, a simulation model using the variation of the temporal signal generated from the QD network was constructed. Figure 5.5 shows a schematic diagram of an information processing system using the randomly distributed QDs. In this scheme, the binary data of the XOR task are encoded as the status of the pulse light of on/off. The encoded pulse sequence is introduced to several areas in the randomly distributed QDs. By optical excitation, fluorescence signals are generated. When a time-sequential input is introduced to the randomly distributed QDs, the responses are modulated according to the energy

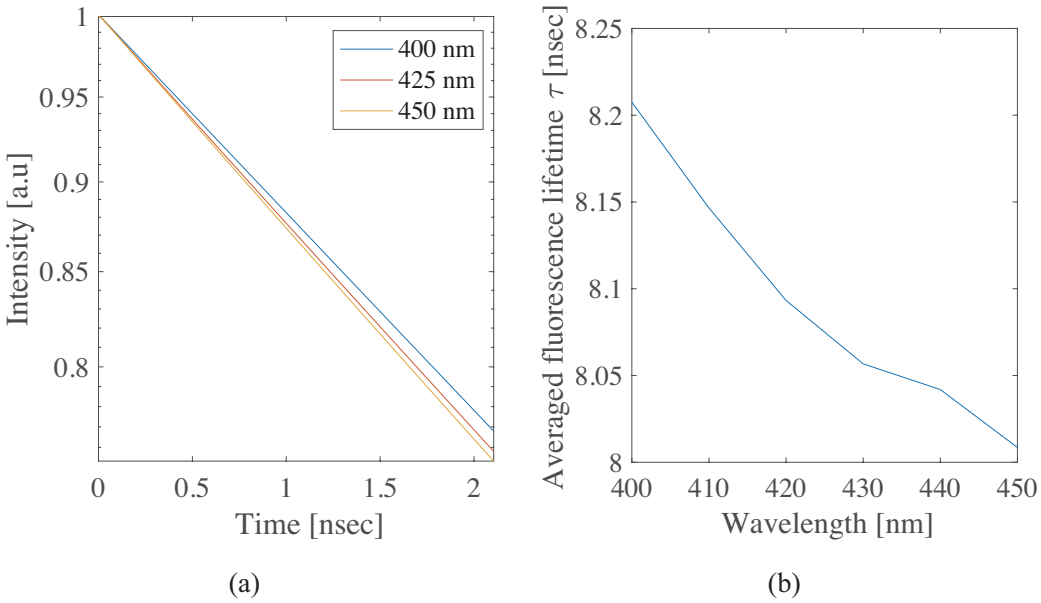

Fig. 5.4 (a) Simulation results of the fluorescence intensity at the irradiation wavelength of the pulse light. The intensity was normalized so that the maximum value is 1. (b) Dependence of the average fluorescence lifetime on the irradiation wavelength.

state of each QD. As a result, fluorescence signals depending on the previous input are obtained, and thus the dynamics of the fluorescence signal can be created. Moreover, the temporal signals generated from individual irradiation areas vary according to the QD distribution, and different types of dynamics can be obtained. The optical input is mapped to the hyperplane based on the dynamics, and the classification of the input data is achievable by linear regression. In this simulation, temporal signals generated from the QD network were estimated under the conditions shown in Fig. 5.2. The weights to individual signals were optimized using Ridge regression. The number of values detected for training was 900, 25% of which were used as test data. The simulation using different QD networks was run 100 times.

Figure 5.6 shows the output of the test data and the label data in the 2-bit XOR task. The irradiation intensity and the irradiation wavelength was 2.8×10^8 W/cm and 400 nm, respectively. The time resolution of the temporal signal and time interval between pulses were set to be 2.5 ns. The number of temporal signals used for the prediction was 20. In response to the transmission of the label data between 0 and 1, the prediction output increased and decreased. The results show that the QD network system can predict the 2-bit XOR data. To evaluate the accuracy, the prediction signal was binarized with the mean value of the prediction output when train data were input. The mean accuracy rate was 95.7%, which is higher than that by the analysis using mere linear regression

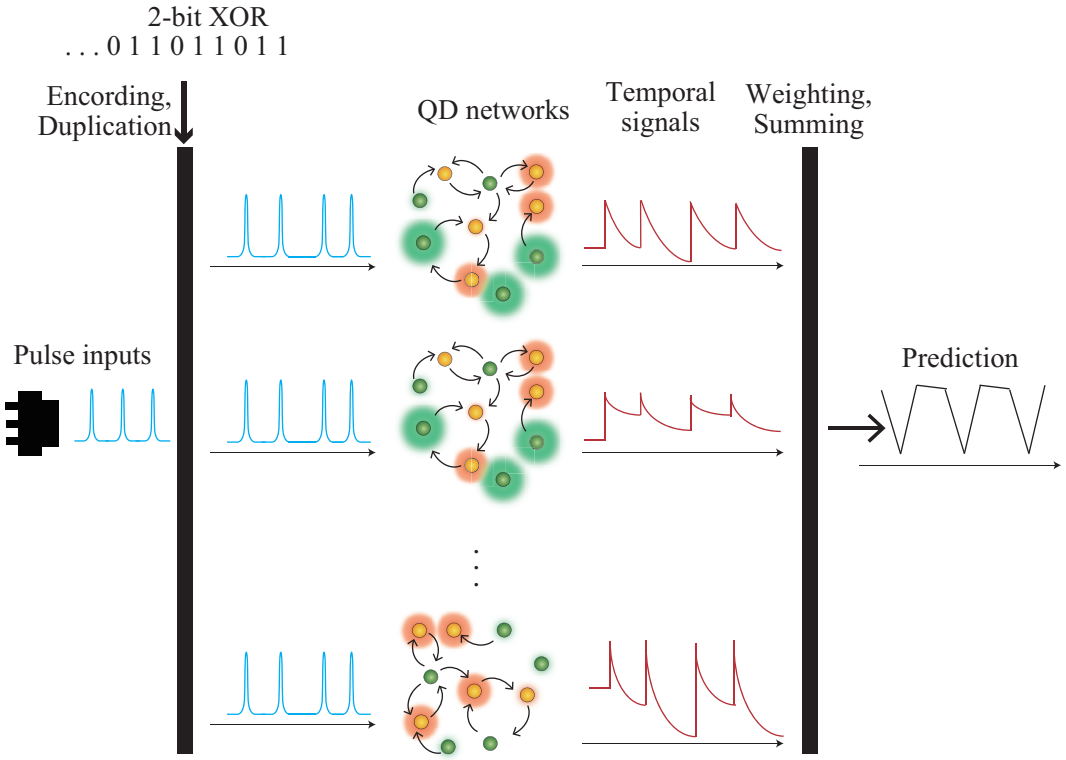

Fig. 5.5 Schematic diagram of temporal information processing system using QD network.

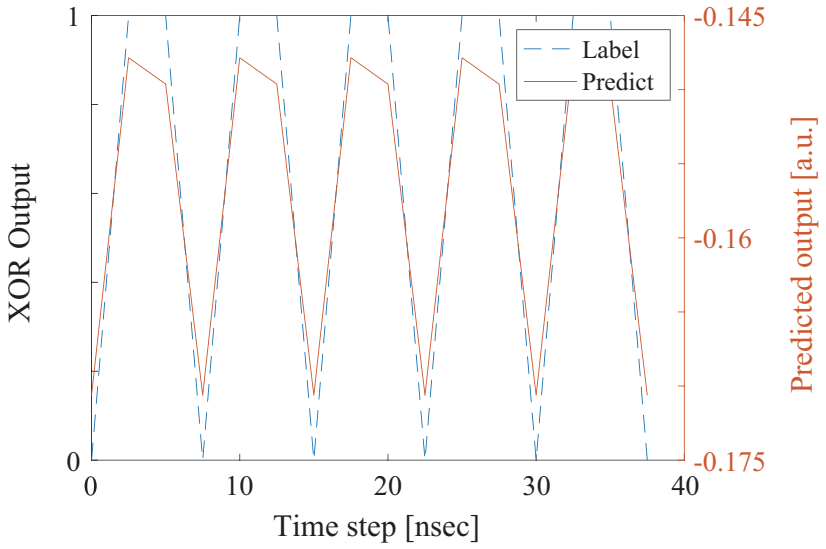

Fig. 5.6 The prediction output of the proposed system and the label data of 2-bit XOR task.

(maximum accuracy rate: 75%) [99]. This shows that the signal dynamics generated from the QD network can be used as temporal information processing. Figure 5.7 shows the relationship between the number of temporal signals used for the prediction and the mean accuracy rate. The time interval between the pulse and time resolution of the detection were set to be 1.0 ns. When the number of temporal signals increases, the accuracy rate is increased. The results indicate that the accuracy rate can be increased by using various types of dynamics from the QD network. The change of the amplification rate of irradiation intensity also increases the accuracy rate to 99.7%. The previous result presented in Section 5.3 shows that a high intensity creates greater variation of temporal signal. This means that more different dynamics can be created at each irradiation area. Therefore, signal modulation depending on the irradiation intensity generates different kinds of temporal signal and improves the accuracy rate.

Next, the relationship between the accuracy and the time interval between encoded pulse light was investigated. The dependence of the test accuracy rate on the time interval between pulses is shown in Figure 5.8. The number of temporal signals used for the prediction was 10. When the interval is 2.5 ns, the accuracy rate is the highest at each amplification rate. The signal modulation by the QD network depends on the energy state of QDs, and the modulation degree decreases as the change of the state is low. When the irradiation interval is 1.0 ns, the individual QDs in the network maintain high energy states. As a result, the variation of dynamics decreases and the accuracy deteriorates. In the case of a long interval of more than 5.0 ns, the energy of the QDs returns to the

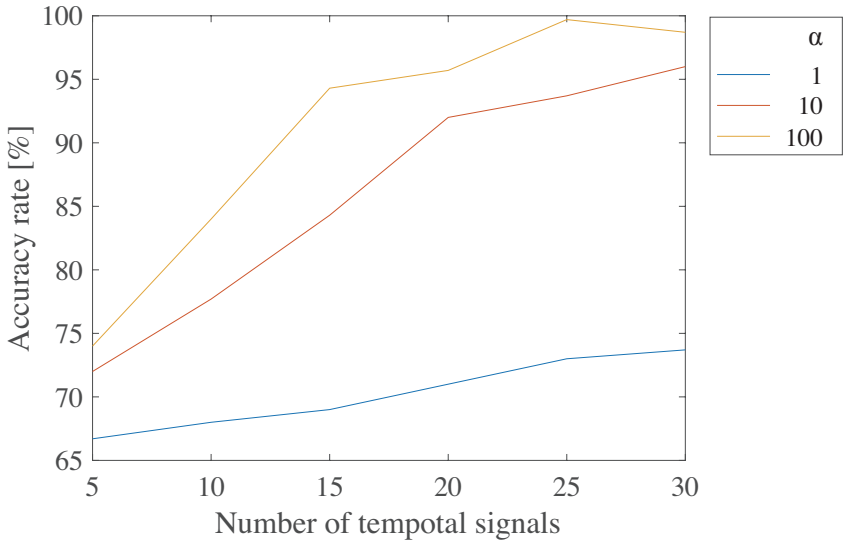

Fig. 5.7 The relationship between the number of simulated signals and the accuracy rate of test data. For each value, α indicates the amplification rate of the irradiation intensity.

initial state before the next pulse light is input and the modulation degree decreases. It is revealed that the encoded pulses with a time interval of 2.5 ns make the best use of the signal modulation of the QD network for improving the prediction result.

5.5 Discussion

The results indicate that a QD network is useful for temporal information processing. The size of the QD network is assumed to be on the nanometer scale, and various temporal signals can be generated by changing the irradiation position. The signal diversity on the nanometer scale provides the miniaturization of the system. Moreover, the temporal signal modulation depending on the irradiation intensity contributes to create more types of dynamics and improves the accuracy. Therefore, the optical conditions are essential for the prediction. In other words, optical control has the potential to optimize the QD network system to the task. These capabilities of QD networks should be effective to process various time-series data.

5.6 Conclusion

In this chapter, the possibility of temporal information processing using a QD network is presented. The mathematical model of the QD network was constructed, and the temporal signals were calculated. The simulation results of temporal signal depending on

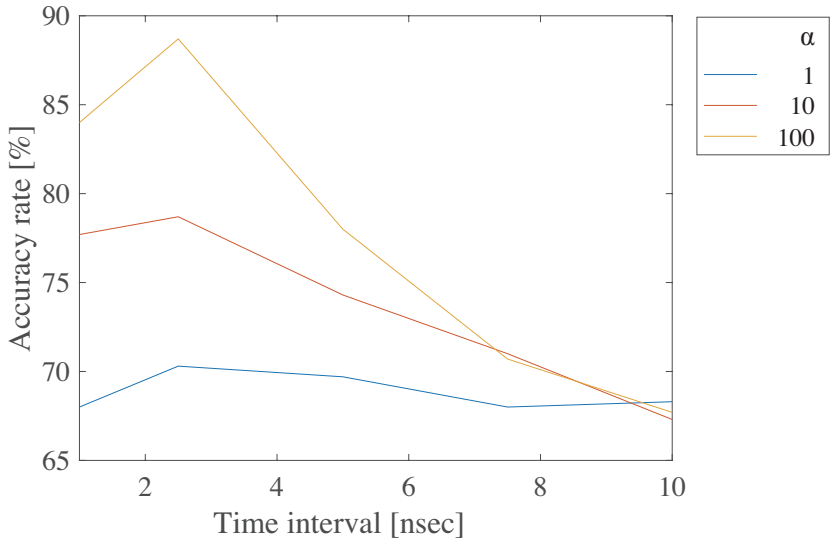

Fig. 5.8 Dependence of the accuracy rate on the time interval between encoded pulse light. α indicates the amplification rate of the irradiation intensity.

the irradiation intensity and wavelength can reproduce the experimental results as shown in Section 4.4. By using the temporal signals, the time-series data of the 2-bit XOR task could be predicted with 95% accuracy. Depending on the irradiation conditions, the temporal signals were modulated and the accuracy rate could increase to 99.7%. The dynamic signal of fluorescence generated from the QD network is essential for the prediction of temporal data.

Conclusion

In this dissertation, the photofunctional nano-object network and its applications were presented. The use of light enabled the induction of reactions between nano-objects at desired times and spaces, and unique functions of the network could be obtained. In this research, two types of photofunctional nano-object network were constructed and their feasibility was demonstrated.

Chapter 1 reviewed the properties of nano-objects and previous research related to nano-object networks. Two types of useful nano-object, DNA and QDs, were introduced and their applications were described. The diverse functions obtained by construction of the network structure and its limitation were also explained. It was shown that optical methods enable the induction of reactions of nano-objects and activation of the function of the nano-object network at desired time and space. The concept and features of the photofunctional nano-object network were described. The purpose of this dissertation was presented, and the research topics to demonstrate the validity of the photofunctional nano-object network were shown.

Chapters 2 and 3 described physical processing by a spatial structure change of nano-object networks constructed by chemical reaction. Optical construction of a DNA gel, which is a typical example of a DNA network, and an application to modify the mobility of micrometer-sized objects were presented. The control of DNA gels' shape enabled a change in their physical properties such as viscosity, allowing modification of the objects' behavior.

Chapter 2 presented microscale patterning of DNA gels by photo-induced self-assembly of DNA. By using thermal energy via a nonradiative relaxation process of excited quenchers, DNA molecules react with each other upon light irradiation and DNA gels consequently form. The experimental results revealed that the DNA gels formed according to the light intensity distribution, and high-intensity light of more than 2.1×10^3 W/cm^2 caused the formation of DNA gels with an unexpected structure. The patterning of DNA gels with an overall size of 70 μm by irradiation of the light pattern was demonstrated. This method enables the formation of DNA gels with desired shapes in a flexible manner and the achievement of physical processing using DNA gels on a microscale.

Chapter 3 described modification of the mobility of a micrometer-sized object by using optical decomposition of DNA gels, as a demonstration of physical processing using a photofunctional DNA network. The spatial decomposition of the DNA gels was imple-

mented on the scale of a few microns with light pattern irradiation. The irradiated light with intensity of 617.3 W/cm^2 decreased the DNA gels' viscosity with 3.0 mPa·s to 1.0 mPa·s, and the mean square displacement of beads encapsulated in the DNA gels could increase by a factor of 3.0. This method provides a new approach for controlling the motion of micrometer-sized objects.

The change of state of DNA networks via optical control enables modulation of the mobility of micrometer-sized objects selectively, dynamically, and remotely. The combination of methods for the formation and decomposition of DNA gels will allow the spatial control of viscosity. DNA gels are biocompatible and control of their viscosity is useful for manipulating and arranging cells. It is expected that these techniques will be applied for the construction of cellular tissues with complicated structures on the microscale and for analyzing the motion of cells.

Chapters 4 and 5 described information processing using nano-object network constructed by physical interaction depending on the optical inputs. In these chapters, the construction of a QD network by optical signaling and the ability to use it in temporal data prediction were presented. By constructing the QD network, the energy state of QDs in the network was modulated dynamically due to multistep FRET and the level occupancy effect, and variations of a signal in time and wavelength domains were created. This diversity has the potential to be used for mapping an optical input to a hyperplane, which enables the handling of complicated information such as time-series data.

Chapter 4 describes the generation of diverse signals by the construction of a QD network. In the experiment, owing to the multistep FRET in QD aggregation, various spectral signals could be generated at different irradiation areas. The temporal signals generated from the QD ensemble were modulated depending on the irradiation intensity. The average fluorescence lifetime of the generated signal decay decreased to one-quarter when the irradiation intensity increased by a factor of 3.0. When the irradiation wavelength was 400 nm, the fluorescence decay was 0.68, which is three times larger than that when the wavelength was 450 nm. The modulation was induced by the level occupancy effect and the change of FRET pathways depending on each optical condition. This method provides diversity of signals in time and wavelength domains by distributing QDs randomly.

Chapter 5 described the possibility of performing temporal information processing using QD networks. A mathematical model considering the FRET and level occupancy effect was constructed. The simulation results could reproduce the experimental results qualitatively. Moreover, the variation of the fluorescence lifetime derived from the network structure increased two times when the irradiation intensity increased 100 times. Using the temporal signals, the prediction of 2-bit XOR data could be achieved with an accuracy rate of 95.7%. Moreover, modulation of the temporal signal depending on the irradiation intensity increased the accuracy rate to 99.7%. These results show that QD

networks have the potential to process temporal information on the nanoscale.

The dynamics of the fluorescence signal generated from the QD network is created by distributing several QDs randomly. The information processing system using the QD network can be constructed on the nanoscale without complicated techniques for QD arrangements. Furthermore, the use of spectral signals expands the variation of the dynamics, and contributes to handling more complicated information. This technique will be applied to advanced information processing such as reservoir computing, which requires the dynamics depending on the sequential input [100]. As shown in Chapter 5, the QD network has both function and potential for realizing reservoir computing. Reservoir computing using QD networks and optical signals provides high-speed processing of temporal data.

The two types of photo-functional nano-object network can also be combined. Specifically, QD networks can be constructed in DNA networks by attaching QDs to DNA. By changing the structure of DNA networks according to optical signals, the fluorescence signals from these networks can be modulated because the distances between QDs attached to DNAs change. This function is useful for further signal modulation according to the input signals and for measuring environmental change corresponding to the structural change of a designed DNA network. It is expected that the combination of photo-functional nano-object networks will confer new abilities on the networks.

So far, the function of nano-object networks has been limited by their pre-designed reaction schemes. The research results obtained here show that the function of nano-object networks can be activated by optical control at the desired time and space, and that their abilities can be expanded by constructing photofunctional nano-object networks.

Future potential work based on this research is presented below. Viscosity control of DNA networks requires the combination of formation and decomposition in response to individual optical signals. By using two types of quencher excited by irradiated light with different wavelengths, it should be possible to increase and decrease the viscosity depending on the irradiation wavelength and to spatially control the mobility of micrometer-sized objects. For building a temporal data processing system using a QD network, it is necessary to construct the optical set-up, which is considered in the simulation. In the generation of sequential pulses encoding an input signal, the use of a resonator and a spatial light modulator is an effective approach. Furthermore, the prediction of more complicated temporal data such as a chaotic signal requires various dynamics. For the generation of signals with various types of dynamics, it is necessary to consider a method for distributing QDs and the types of QDs to be used for a QD network.

The use of nano-objects on the microscale and nanoscale is still challenging, but has the potential to reveal unknown phenomena and to build innovative information processing systems. Photofunctional nano-object networks expand the potential of nano-objects. The achievements presented in this dissertation show the availability of photofunctional

nano-object networks, and the fundamental techniques can be applied to a wide range of fields including biology, physics, and engineering.

Appendix

QD parameter for the simulation in Chapter 5

Parameters for QD_D and QD_A are determined as the experimentally measured values for QD540 and of QD580. Quantum yield was set, for both QD, to be 0.4 which is the minimum value of the employed QDs described in the technical specifications [101]. The saturation intensity of each QD, I_{sat}, was obtained from the equation in the previous research [64]. The overlap integral to obtain Förester distance R_0 is calculated using the absorption cross sections and normalized fluorescence spectrum shown in Fig. 5.9.

Table 5.1 QD parameters in the simulation

Type	Parameter	Value
QD_D	Q_D	0.40
	τ_D	8.6 [ns]
	ν_D	5.6×10^{14} [Hz]
	$k_r = Q/\tau_D$	4.7×10^7
	$k_{nr} = (1-Q)/\tau_D$	7.0×10^7
	$I_{sat} = h\nu_D/\tau_D\sigma_D$	2.8×10^6 [W/cm^2]
	$N = 1/\tau_D$	1.2×10^8
	R_0 $(QD_D \rightarrow QD_D)$	4.6 [nm]
	R_0 $(QD_D \rightarrow QD_A)$	7.3 [nm]

Type	Parameter	Value
QD_A	Q_A	0.40
	τ_A	7.9 [ns]
	ν_A	5.2×10^{14} [Hz]
	$k_r = Q_A/\tau_A$	5.1×10^7
	$k_{nr} = (1-Q_A)/\tau_A$	7.6×10^7
	$I_{sat} = h\nu_A/\tau_A\sigma_A$	3.3×10^6 [W/cm^2]
	$N = 1/\tau_A$	1.3×10^8
	R_0 $(QD_A \rightarrow QD_D)$	6.1 [nm]
	R_0 $(QD_A \rightarrow QD_A)$	6.9 [nm]

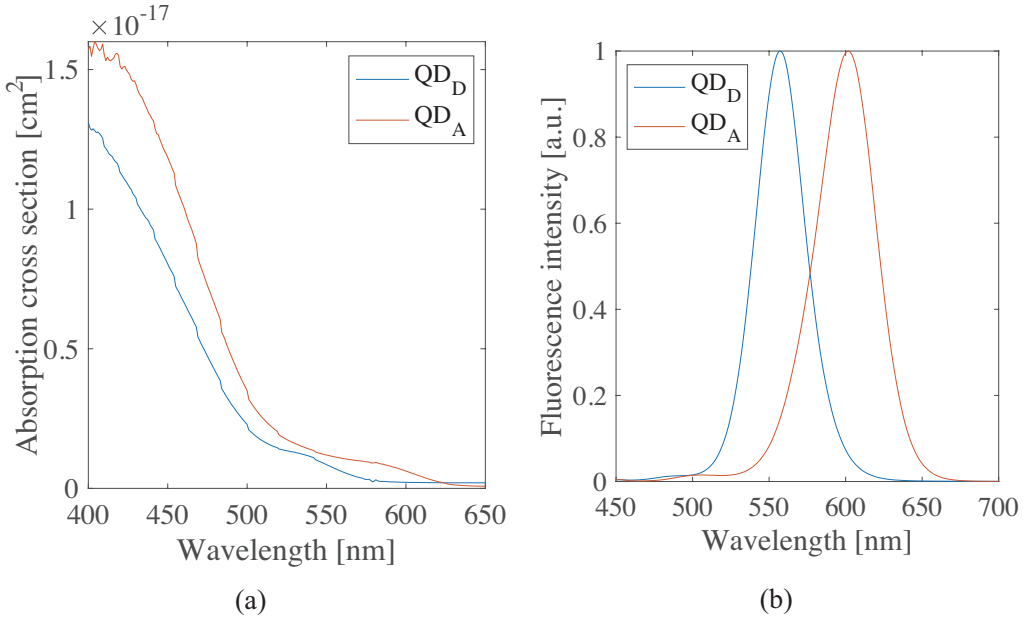

Fig. 5.9 (a) Absorption cross-section of each QD depending on the irradiation wavelength . (b) Fluorescence and fluorescence spectra of individual QDs.

Bibliography

[1] J. Wang, J. Chao, H. Liu, S. Su, L. Wang, W. Huang, I. Willner, and C. Fan, "Clamped Hybridization Chain Reactions for the Self-Assembly of Patterned DNA Hydrogels," Angewandte Chemie - International Edition **56**, 2171–2175 (2017).

[2] H. J. Cleaves, "Watson–Crick Pairing," Encyclopedia of Astrobiology, pp. 1775–1776 (2011).

[3] F. Crick and J. Watson, "Molecular Structure of Nucleic Acids: A Structure for Deoxyribose Nucleic Acid," Nature volume **171**, 737—-738 (1953).

[4] M. Mandelkern, J. G. Elias, D. Eden, and D. M. Crothers, "The dimensions of DNA in solution," Journal of Molecular Biology **152**, 153–161 (1981).

[5] J. SantaLucia, "A unified view of polymer, dumbbell, and oligonucleotide DNA nearest-neighbor thermodynamics," Proceedings of the National Academy of Sciences of the United States of America **95**, 1460–1465 (1998).

[6] N. Sugimoto, S. I. Nakano, M. Yoneyama, and K. I. Honda, "Improved thermodynamic parameters and helix initiation factor to predict stability of DNA duplexes," Nucleic Acids Research **24**, 4501–4505 (1996).

[7] M. Zuker, "Mfold web server for nucleic acid folding and hybridization prediction," Nucleic Acids Research **31**, 3406–3415 (2003).

[8] J. N. Zadeh, C. D. Steenberg, J. S. Bois, B. R. Wolfe, M. B. Pierce, A. R. Khan, R. M. Dirks, and N. A. Pierce, "Software News and Updates NUPACK: Analysis and Design of Nucleic Acid Systems," Journal of computational chemistry **28**, 73–86 (2009).

[9] A. Currin, K. Korovin, M. Ababi, K. Roper, D. B. Kell, P. J. Day, and R. D. King, "Computing exponentially faster: Implementing a non-deterministic universal Turing machine using DNA," Journal of the Royal Society Interface **14**, 20160990 (2017).

[10] L. M. Adleman, "Molecular computation of solutions to combinatorial problems," Science **266**, 1021–1024 (1994).

[11] S. Ogasawara and K. Fujimoto, "Solution of a SAT Problem on a Photochemical DNA Computer," Chemistry Letters **34**, 378–379 (2005).

[12] D. Mariottini, A. Idili, A. Vallée-Bélisle, K. W. Plaxco, and F. Ricci, "A DNA Nanodevice That Loads and Releases a Cargo with Hemoglobin-Like Allosteric Control and Cooperativity," Nano Letters **17**, 3225–3230 (2017).

[13] T. G. Drummond, M. G. Hill, and J. K. Barton, "Electrochemical DNA sensors," Nature Biotechnology **21**, 1192–1199 (2003).

[14] N. C. Harris and C. H. Kiang, "Disorder in DNA-linked gold nanoparticle assemblies," Physical Review Letters **95**, 1–4 (2005).

[15] D. P. Bratu, B. J. Cha, M. M. Mhlanga, F. R. Kramer, and S. Tyagi, "Visualizing the distribution and transport of mRNAs in living cells," Proceedings of the National Academy of Sciences of the United States of America **100**, 13308–13313 (2003).

[16] J. Schnitzbauer, M. T. Strauss, T. Schlichthaerle, F. Schueder, and R. Jungmann, "Super-resolution microscopy with DNA-PAINT," Nature Protocols **12**, 1198–1228 (2017).

[17] J. M. Brockman, H. Su, A. T. Blanchard, Y. Duan, T. Meyer, M. E. Quach, R. Glazier, A. Bazrafshan, R. L. Bender, A. V. Kellner, H. Ogasawara, R. Ma, F. Schueder, B. G. Petrich, R. Jungmann, R. Li, A. L. Mattheyses, Y. Ke, and K. Salaita, "Live-cell super-resolved PAINT imaging of piconewton cellular traction forces," Nature Methods **17**, 1018–1024 (2020).

[18] M. Grabolle, J. Ziegler, A. Merkulov, T. Nann, and U. Resch-Genger, "Stability and fluorescence quantum yield of CdSe-ZnS quantum dots - Influence of the thickness of the ZnS shell," Annals of the New York Academy of Sciences **1130**, 235–241 (2008).

[19] T. M. Jovin, "Quantum dots finally come of age," Nature Biotechnology **21**, 32–33 (2003).

[20] A. P. Alivisatos, "Semiconductor clusters, nanocrystals, and quantum dots," Science **271**, 933–936 (1996).

[21] W. W. Yu, L. Qu, W. Guo, and X. Peng, "Experimental determination of the extinction coefficient of CdTe, CdSe, and CdS nanocrystals," Chemistry of Materials **15**, 2854–2860 (2003).

[22] H. K. Jun, M. A. Careem, and A. K. Arof, "Quantum dot-sensitized solar cells-perspective and recent developments: A review of Cd chalcogenide quantum dots as sensitizers," Renewable and Sustainable Energy Reviews **22**, 148–167 (2013).

[23] B. Bajorowicz, M. P. Kobylański, A. Gołąbiewska, J. Nadolna, A. Zaleska-Medynska, and A. Malankowska, "Quantum dot-decorated semiconductor micro- and nanoparticles: A review of their synthesis, characterization and application in photocatalysis," Advances in Colloid and Interface Science **256**, 352–372 (2018).

[24] R. Luchowski, E. Matveeva, I. Gryczynski, E. Terpetschnig, L. Patsenker, G. Laczko, J. Borejdo, and Z. Gryczynski, "Single Molecule Studies of Multiple-Fluorophore Labeled Antibodies. Effect of Homo-FRET on the Number of Photons Available Before Photobleaching," Current Pharmaceutical Biotechnology **9**, 411–420 (2008).

[25] X. Michalet, F. F. Pinaud, L. A. Bentolila, J. M. Tsay, S. Doose, J. J. Li, G. Sun-

daresan, A. M. Wu, S. S. Gambhir, and S. Weiss, "Quantum dots for live cells, in vivo imaging, and diagnostics," Science **307**, 538–544 (2005).

[26] M. E. Åkerman, W. C. Chan, P. Laakkonen, S. N. Bhatia, and E. Ruoslahti, "Nanocrystal targeting in vivo," Proceedings of the National Academy of Sciences of the United States of America **99**, 12617–12621 (2002).

[27] K. F. Chou and A. M. Dennis, "Förster resonance energy transfer between quantum dot donors and quantum dot acceptors," Sensors **15**, 13288–13325 (2015).

[28] A. C. S. Samia, S. Dayal, and C. Burda, "Quantum Dot-based Energy Transfer: Perspectives and Potential for Applications in Photodynamic Therapy," Photochemistry and Photobiology **82**, 617 (2006).

[29] T. Shiraki, Y. Tsuchiya, and S. Shinkai, "Ratiometric fluorescent sensor for 2,4,6-trinitrotoluene designed based on energy transfer between size-different quantum dots," Chemistry Letters **39**, 156–158 (2010).

[30] S. Wang, N. Mamedova, N. A. Kotov, W. Chen, and J. Studer, "Antigen/Antibody Immunocomplex from CdTe Nanoparticle Bioconjugates," Nano Letters **2**, 817–822 (2002).

[31] V. I. Klimov, A. A. Mikhailovsky, S. Xu, A. Malko, J. A. Hollingsworth, C. A. Leatherdale, H. J. Eisler, and M. G. Bawendi, "Optical gain and stimulated emission in nanocrystal quantum dots," Science **290**, 314–317 (2000).

[32] N. C. Seeman, "Nucleic acid junctions and lattices," Journal of Theoretical Biology **99**, 237–247 (1982).

[33] E. Winfree, F. Liu, L. A. Wenzler, and N. C. Seeman, "Design and self-assembly of two-dimensional DNA crystals," Nature **394**, 539–544 (1998).

[34] P. W. Rothemund, "Folding DNA to create nanoscale shapes and patterns," Nature **440**, 297–302 (2006).

[35] C. R. Simmons, F. Zhang, J. J. Birktoft, X. Qi, D. Han, Y. Liu, R. Sha, H. O. Abdallah, C. Hernandez, Y. P. Ohayon, N. C. Seeman, and H. Yan, "Construction and Structure Determination of a Three-Dimensional DNA Crystal," Journal of the American Chemical Society **138**, 10047–10054 (2016).

[36] G. Tikhomirov, P. Petersen, and L. Qian, "Programmable disorder in random DNA tilings," Nature Nanotechnology **12**, 251–259 (2017).

[37] Y. Hao, M. Kristiansen, R. Sha, J. J. Birktoft, C. Hernandez, C. Mao, and N. C. Seeman, "A device that operates within a self-assembled 3D DNA crystal," Nature Chemistry **9**, 824–827 (2017).

[38] F. Hong, F. Zhang, Y. Liu, and H. Yan, "DNA Origami: Scaffolds for Creating Higher Order Structures," Chemical Reviews **117**, 12584–12640 (2017).

[39] K. M. Cherry and L. Qian, "Scaling up molecular pattern recognition with DNA-based winner-take-all neural networks," Nature **559**, 370–388 (2018).

[40] C. Jung, P. B. Allen, and A. D. Ellington, "A stochastic DNA walker that traverses

a microparticle surface," Nature Nanotechnology **11**, 157–163 (2016).

[41] A. J. Thubagere, W. Li, R. F. Johnson, Z. Chen, S. Doroudi, Y. L. Lee, G. Izatt, S. Wittman, N. Srinivas, D. Woods, E. Winfree, and L. Qian, "A cargo-sorting DNA robot," Science **357** (2017).

[42] M. Iwaki, S. F. Wickham, K. Ikezaki, T. Yanagida, and W. M. Shih, "A programmable DNA origami nanospring that reveals force-induced adjacent binding of myosin VI heads," Nature Communications **7**, 1–10 (2016).

[43] E. Kopperger, J. List, S. Madhira, F. Rothfischer, D. C. Lamb, and F. C. Simmel, "A self-assembled nanoscale robotic arm controlled by electric fields," Science **359**, 296–301 (2018).

[44] L. I. Yougen, Y. D. Tseng, S. Y. Kwon, L. D'Espaux, J. S. Bunch, P. L. McEuen, and D. Luo, "Controlled assembly of dendrimer-like DNA," Nature Materials **3**, 38–42 (2004).

[45] S. H. Um, J. B. Lee, N. Park, S. Y. Kwon, C. C. Umbach, and D. Luo, "Enzyme-catalysed assembly of DNA hydrogel," Nature Materials **5**, 797–801 (2006).

[46] Y. Xing, E. Cheng, Y. Yang, P. Chen, T. Zhang, Y. Sun, Z. Yang, and D. Liu, "Self-assembled DNA hydrogels with designable thermal and enzymatic responsiveness," Advanced Materials **23**, 1117–1121 (2011).

[47] E. Cheng, Y. Xing, P. Chen, Yang, Y. Sun, D. Zhou, T. Xu, Q. Fan, and D. Liu, "A pH-triggered, fast-responding DNA hydrogel," Angewandte Chemie - International Edition **48**, 7660–7663 (2009).

[48] W. Guo, X. J. Qi, R. Orbach, C. H. Lu, L. Freage, I. Mironi-Harpaz, D. Seliktar, H. H. Yang, and I. Willner, "Reversible Ag+-crosslinked DNA hydrogels," Chemical Communications **50**, 4065–4068 (2014).

[49] Z. Zhu, C. Wu, H. Liu, Y. Zou, X. Zhang, H. Kang, C. J. Yang, and W. Tan, "An aptamer cross-linked hydrogel as a colorimetric platform for visual detection," Angewandte Chemie - International Edition **49**, 1052–1056 (2010).

[50] L. Zhang, J. Lei, L. Liu, C. Li, and H. Ju, "Self-assembled DNA hydrogel as switchable material for aptamer-based fluorescent detection of protein," Analytical Chemistry **85**, 11077–11082 (2013).

[51] C. Li, A. Faulkner-Jones, A. R. Dun, J. Jin, P. Chen, Y. Xing, Z. Yang, Z. Li, W. Shu, D. Liu, and R. R. Duncan, "Rapid formation of a supramolecular polypeptide-DNA Hydrogel for in situ three-dimensional multilayer bioprinting," Angewandte Chemie - International Edition **54**, 3957–3961 (2015).

[52] P. Song, D. Ye, X. Zuo, J. Li, J. Wang, H. Liu, M. T. Hwang, J. Chao, S. Su, L. Wang, J. Shi, L. Wang, W. Huang, R. Lal, and C. Fan, "DNA Hydrogel with Aptamer-Toehold-Based Recognition, Cloaking, and Decloaking of Circulating Tumor Cells for Live Cell Analysis," Nano Letters **17**, 5193–5198 (2017).

[53] J. Jin, Y. Xing, Y. Xi, X. Liu, T. Zhou, X. Ma, Z. Yang, S. Wang, and D. Liu,

"A triggered DNA hydrogel cover to envelop and release single cells," Advanced Materials **25**, 4714–4717 (2013).

[54] C. R. Kagan, C. B. Murray, M. Nirmal, and M. G. Bawendi, "Electronic energy transfer in CdSe Quantum dot solids," Physical Review Letters **76**, 1517–1520 (1996).

[55] K. Boeneman, D. E. Prasuhn, J. B. Blanco-Canosa, P. E. Dawson, J. S. Melinger, M. Ancona, M. H. Stewart, K. Susumu, A. Huston, and I. L. Medintz, "Self-assembled quantum dot-sensitized multivalent DNA photonic wires," Journal of the American Chemical Society **132**, 18177–18190 (2010).

[56] C. Berger, U. Huttner, M. Mootz, M. Kira, S. W. Koch, J. S. Tempel, M. Aßmann, M. Bayer, A. M. Mintairov, and J. L. Merz, "Quantum-memory effects in the emission of quantum-dot microcavities," Physical Review Letters **113**, 1–5 (2014).

[57] N. Tate, W. Nomura, M. Naruse, T. Kawazoe, T. Yatsui, M. Hoga, Y. Ohyagi, Y. Sekine, H. Fujita, and M. Ohtsu, "Demonstration of Modulatable Nanophotonics based on modulatable optical near-field interactions between dispersed quantum dots," 2011 ICO International Conference on Information Photonics, IP 2011 **19**, 4051–4055 (2011).

[58] N. Tate, Y. Liu, T. Kawazoe, M. Naruse, T. Yatsui, and M. Ohtsu, "Nanophotonic droplet: A nanometric optical device consisting of size- and number-selective coupled quantum dots," Applied Physics B: Lasers and Optics **110**, 293–297 (2013).

[59] C. R. Kagan, E. Lifshitz, E. H. Sargent, and D. V. Talapin, "Building devices from colloidal quantum dots," Science **353** (2016).

[60] Y. Ogura, T. Nishimura, and J. Taniida, "Self-contained photonically-controlled DNA tweezers," Applied Physics Express **2** (2009).

[61] T. Kalkbrenner, M. Ramstein, J. Mlynek, and V. Sandoghdar, "A single gold particle as a probe for apertureless scanning near-field optical microscopy," Journal of Microscopy **202**, 72–76 (2001).

[62] I. L. Medintz and N. Hildebrandt, " FRET-Förster resonance energy transfer: from theory to applications," Wiley-VCH (2013).

[63] A. Gaiduk, M. Yorulmaz, P. V. Ruijgrok, and M. Orrit, "Room-temperature detection of a single molecule's absorption by photothermal contrast," Science **330**, 353–356 (2010).

[64] Y. Ogura, A. Onishi, T. Nishimura, and J. Tanida, "Optically controlled release of DNA based on nonradiative relaxation process of quenchers," Biomedical Optics Express **7**, 2142 (2016).

[65] T. Nishimura, R. Fujii, Y. Ogura, and J. Tanida, "Optically controllable molecular logic circuits," Applied Physics Letters **107** (2015).

[66] M. Massey, M. G. Ancona, I. L. Medintz, and W. R. Algar, "Time-Gated DNA Photonic Wires with Förster Resonance Energy Transfer Cascades Initiated by a

Luminescent Terbium Donor," ACS Photonics **2**, 639–652 (2015).

[67] Y. S. Park, W. K. Bae, T. Baker, J. Lim, and V. I. Klimov, "Effect of Auger Recombination on Lasing in Heterostructured Quantum Dots with Engineered Core/Shell Interfaces," Nano Letters **15**, 7319–7328 (2015).

[68] V. I. Klimov, A. A. Mikhailovsky, D. W. McBranch, C. A. Leatherdale, and M. G. Bawendi, "Quantization of multiparticle Auger rates in semiconductor quantum dots," Science **287**, 1011–1014 (2000).

[69] T. Kawazoe, M. Ohtsu, S. Aso, Y. Sawado, Y. Hosoda, K. Yoshizawa, K. Akahane, N. Yamamoto, and M. Naruse, "Two-dimensional array of room-temperature nanophotonic logic gates using InAs quantum dots in mesa structures," Applied Physics B: Lasers and Optics **103**, 537–546 (2011).

[70] M. Beutler, K. Makrogianneli, R. J. Vermeij, M. Keppler, T. Ng, T. M. Jovin, and R. Heintzmann, "satFRET: Estimation of Förster resonance energy transfer by acceptor saturation," European Biophysics Journal **38**, 69–82 (2008).

[71] E. M. Willner, Y. Kamada, Y. Suzuki, T. Emura, K. Hidaka, H. Dietz, H. Sugiyama, and M. Endo, "Single-Molecule Observation of the Photoregulated Conformational Dynamics of DNA Origami Nanoscissors," Angewandte Chemie - International Edition **56**, 15324–15328 (2017).

[72] T. Nishimura, Y. Ogura, and J. Tanida, "Reusable molecular sensor based on photonic activation control of DNA probes," Biomedical Optics Express **3**, 920 (2012).

[73] G. Pardatscher, M. Schwarz-Schilling, S. S. Daube, R. H. Bar-Ziv, and F. C. Simmel, "Gene Expression on DNA Biochips Patterned with Strand-Displacement Lithography," Angewandte Chemie - International Edition **57**, 4783–4786 (2018).

[74] N. Park, S. H. Um, H. Funabashi, J. Xu, and D. Luo, "A cell-free protein-producing gel," Nature Materials **8**, 432–437 (2009).

[75] S. Shimomura, T. Nishimura, Y. Ogura, and J. Tanida, "Photothermal fabrication of microscale patterned DNA hydrogels," Royal Society Open Science **5** (2018).

[76] S. Shimomura, T. Nishimura, Y. Ogura, and J. Tanida, "Optical decomposition of DNA gel and modification of object mobility on micrometre scale," Scientific Reports **9**, 1–5 (2019).

[77] S. Shimomura, T. Nishimura, Y. Miyata, N. Tate, Y. Ogura, and J. Tanida, "Spectral and temporal optical signal generation using randomly distributed quantum dots," Optical Review **27**, 264–269 (2020).

[78] J. B. Lee, S. Peng, D. Yang, Y. H. Roh, H. Funabashi, N. Park, E. J. Rice, L. Chen, R. Long, M. Wu, and D. Luo, "A mechanical metamaterial made from a DNA hydrogel," Nature Nanotechnology **7**, 816–820 (2012).

[79] D. Kandatsu, K. Cervantes-Salguero, I. Kawamata, S. Hamada, S. i. M. Nomura, K. Fujimoto, and S. Murata, "Reversible Gel–Sol Transition of a Photo-Responsive DNA Gel," ChemBioChem **1292**, 1118–1121 (2016).

[80] J. R. Fienup, "Phase retrieval algorithms: a comparison," Applied Optics **21**, 2758 (1982).

[81] S. A. Marras, F. R. Kramer, and S. Tyagi, "Efficiencies of fluorescence resonance energy transfer and contact-mediated quenching in oligonucleotide probes." Nucleic acids research **30**, 1–8 (2002).

[82] J. T. Edward, "Molecular volumes and the Stokes-Einstein equation," Journal of Chemical Education **47**, 261–270 (1970).

[83] J. Bao and M. G. Bawendi, "A colloidal quantum dot spectrometer," Nature **523**, 67–70 (2015).

[84] D. Bera, L. Qian, T. K. Tseng, and P. H. Holloway, "Quantum dots and their multimodal applications: A review," Materials **3**, 2260–2345 (2010).

[85] L. Zhang, C. Chen, W. Li, G. Gao, P. Gong, and L. Cai, "Living Cell Multilifetime Encoding Based on Lifetime-Tunable Lattice-Strained Quantum Dots," ACS Applied Materials and Interfaces **8**, 13187–13191 (2016).

[86] J. C. Claussen, W. R. Algar, N. Hildebrandt, K. Susumu, M. G. Ancona, and I. L. Medintz, "Biophotonic logic devices based on quantum dots and temporally-staggered Förster energy transfer relays," Nanoscale **5**, 12156–12170 (2013).

[87] J. C. Claussen, N. Hildebrandt, K. Susumu, M. G. Ancona, and I. L. Medintz, "Complex logic functions implemented with quantum dot bionanophotonic circuits." ACS applied materials & interfaces **6**, 3771–3778 (2014).

[88] S. M. Hendrickson, C. N. Weiler, R. M. Camacho, P. T. Rakich, A. I. Young, M. J. Shaw, T. B. Pittman, J. D. Franson, and B. C. Jacobs, "All-optical-switching demonstration using two-photon absorption and the Zeno effect," Physical Review A - Atomic, Molecular, and Optical Physics **87**, 1–5 (2013).

[89] D. Sridharan and E. Waks, "All-optical switch using quantum-dot saturable absorbers in a DBR microcavity," IEEE Journal of Quantum Electronics **47**, 31–39 (2011).

[90] S. S. Li, Semiconductor Physical Electronics (2006).

[91] H. Jaeger, "The " echo state " approach to analysing and training recurrent neural networks – with an Erratum note 1," German National Research Center for Information Technology, GMD Technical Report **148**, 13 (2001).

[92] M. Nakagawa, Y. Miyata, N. Tate, T. Nishimura, S. Shimomura, S. Shirasaka, J. Tanida, and H. Suzuki, "Spatiotemporal model for fret networks with multiple donors and acceptors: multicomponent exponential decay derived from the master equation," Journal of the Optical Society of America B **38**, 294–299 (2021).

[93] F. V. De Sales, J. M. Cruz, S. W. Da Silva, M. A. Soler, P. C. Morais, M. J. Da Silva, A. A. Quivy, and J. R. Leite, "Coupled rate equation modeling of self-assembled quantum dot photoluminescence," Microelectronics Journal **34**, 705–707 (2003).

[94] A. Zrenner, E. Beham, S. Stufler, F. Findeis, M. Bichler, and G. Abstreiter, "Coher-

ent properties of a two-level system based on a quantum-dot photodiode," Nature **418**, 612–614 (2002).

[95] I. O'Driscoll, P. Blood, and P. M. Smowton, "Rate equation analysis of quantum dot population in InAs/GaAs laser structures," Optics InfoBase Conference Papers pp. 14–15 (2010).

[96] H. M. Watrob, C. P. Pan, and M. D. Barkley, "Two-step FRET as a structural tool," Journal of the American Chemical Society **125**, 7336–7343 (2003).

[97] F. Laporte, A. Katumba, J. Dambre, and P. Bienstman, "Numerical demonstration of neuromorphic computing with photonic crystal cavities," Optics Express **26**, 7955 (2018).

[98] F. D. L. Coarer, M. Sciamanna, A. Katumba, M. Freiberger, J. Dambre, P. Bienstman, and D. Rontani, "All-Optical Reservoir Computing on a Photonic Chip Using Silicon-Based Ring Resonators," IEEE Journal of Selected Topics in Quantum Electronics **24** (2018).

[99] K. Vandoorne, P. Mechet, T. Van Vaerenbergh, M. Fiers, G. Morthier, D. Verstraeten, B. Schrauwen, J. Dambre, and P. Bienstman, "Experimental demonstration of reservoir computing on a silicon photonics chip," Nature Communications **5**, 1–6 (2014).

[100] G. Tanaka, T. Yamane, J. B. Héroux, R. Nakane, N. Kanazawa, S. Takeda, H. Numata, D. Nakano, and A. Hirose, "Recent advances in physical reservoir computing: A review," Neural Networks **115**, 100–123 (2019).

[101] NN-labs, "Technical specifications," `https://www.optosirius.co.jp/NN-Labs/techspec.html`